photonics

MDPI

Article

Symmetry Considerations Regarding the Optimal Design of Non-Hermitian Complex-Coupled DFB Lasers

Yaoyao Liang [1,†], Yara El Droubi [1], Henri Benisty [2], Abderrahim Ramdane [1] and Anatole Lupu [1,*]

[1] Centre de Nanosciences et de Nanotechnologies, CNRS, Université Paris-Saclay, C2N– 10 Boulevard Thomas Gobert, 91120 Palaiseau, France
[2] Laboratoire Charles Fabry, Université Paris-Saclay, Institut d'Optique IOGS, 2 Avenue A Fresnel, 91120 Palaiseau, France
* Correspondence: anatole.lupu@c2n.upsaclay.fr
† Current address: Quantum Science Center of Guangdong-HongKong-Macao Greater Bay Area, Shenzhen 518000, China.

Abstract

This work focuses on the design of non-Hermitian DFB lasers incorporating phase-shifted dielectric and metallic gratings, emphasizing the symmetry aspects of the complex refractive index profile. Conventional DFB lasers featuring dielectric Bragg gratings and metallic gratings are also investigated. The impact of the phase shift between the gratings, as well as facet boundary conditions, was analyzed in terms of threshold gain and gain contrast relative to the next-higher-order laser pole. Significant performance improvements were predicted for complex-coupled DFB lasers wherein the dielectric and metallic gratings are either in-phase or out-of-phase. In contrast, for PT-symmetric configurations, we found that reflection asymmetry, which was expected to further enhance DFB laser performance, is compromised by facet reflections. To address this issue, lasing must occur at the Bragg wavelength, and the contribution of the PT-symmetry-induced asymmetric reflection must be enhanced. The solution involves using high-reflectivity and anti-reflective facet coatings. Modeling results show a threshold gain as low as 26 dB/cm, with laser emission occurring exactly at the Bragg wavelength. The gain contrast relative to the next-higher mode reached 72 dB/cm. Such gain contrast should ensure extremely robust single-mode laser operation. These results also suggest better tolerance of optical feedback and, as a potential outcome, operation without an optical isolator.

Keywords: non-Hermitian photonics; DFB laser; complex-coupled Bragg gratings; Parity-Time symmetry; single-wavelength laser emission; threshold gain; optical return loss tolerance; isolator-free operation

Check for updates

Received: 10 August 2026
Revised: 14 September 2026
Accepted: 17 September 2026
Published: 30 September 2026

Copyright: © 2026 by the authors. Licensee MDPI, Basel, Switzerland. This article is an open access article distributed under the terms and conditions of the Creative Commons Attribution (CC BY) license.

1. Introduction

The continued growth of the Internet and increases in data exchange traffic have generated a multi-billion-dollar global market for optoelectronic components used for the emission, transmission, and reception of optical signals and their conversion into electronic format. Distributed feedback (DFB) laser diodes account for the largest share of the telecommunications laser diode market, amounting to approximately USD 2.15 billion in 2024, with the sector exhibiting a robust growth trajectory. The market is expected to expand at a compound annual growth rate of 8.7%, culminating in a projected value of USD 4.49 billion by 2033 [1].

One of the key challenges regarding index-coupled DFB lasers is achieving single-frequency operation, specifically emission in a single longitudinal mode of the laser cavity. A significant proportion of manufactured laser diodes exhibit dual-mode frequency behavior. The phase-shifted DFB laser, featuring a $\lambda/4$ phase shift at the center of the grating (analogous to a defect mode or cavity mode), is the conventional solution to this problem. It produces a mode exactly at the Bragg frequency, provided the facets are perfectly anti-reflection (AR)-coated. However, these lasers suffer from several main limitations:

- Specific, complex techniques are required to implement the phase shift at the center of the Bragg grating (BG).
- Spatial hole burning (depletion of charge carriers, specifically holes, within the laser cavity) leads to reduced single-frequency performance at high coupling coefficients [2].
- Single-frequency performance degrades significantly with imperfect AR coatings [3].

It has been known since Yariv's seminal papers in the late 1970s that imaginary-index modulation naturally yields single-mode behavior. In purely index-coupled (IC-DFB) lasers, only the real part of the refractive index is modified, resulting in a real coupling coefficient κ. Conversely, in purely gain-coupled (GC-DFB) lasers (or loss-coupled DFB lasers), the imaginary part of the index, such as the gain or loss, is modified, yielding an imaginary κ value. Successful attempts to implement a grating with a modulated imaginary component were made in the 1990s (at Bell Labs and NTT), leading to the development of gain-coupled or, more generally, complex-coupled DFB lasers. Given their superior immunity to facet reflections, it was reasonable to expect reduced sensitivity to optical feedback [4,5]. It was also observed that this sensitivity decreases as the coupling strength, κ, increases. However, achieving complex modulation solely by modulating the laser core, specifically the active layer (e.g., multiple quantum wells), proved impractical. Not only was the modulation weak, but the device's efficiency suffered because of the adverse impact on electronic properties.

Consequently, achieving sufficiently strong imaginary modulation required an absorbing grating located outside the active region. For instance, coupling coefficients of approximately 5–20 cm^{-1} were achieved using a chromium grating [6] ($\kappa L \approx 0.25$ for 500 μm long DFB lasers). However, such high loss modulation also increases average losses, thereby increasing noise [7], necessitating higher gain levels, and raising the threshold current density [8]. Moreover, the proper operation of laser diodes can be severely disrupted by optical feedback (i.e., reflections along the optical path), leading to degradation in system transmission performance [9]. Immunity to such disturbances is typically ensured by garnet-based (magneto-)optical isolators integrated into transmitter modules between the laser diode and fiber. However, this entails significant costs for high-data-rate metropolitan and local area networks. A highly desirable alternative would be isolator-free laser assemblies—if lasers with high tolerance to optical feedback were available. The quest for an isolator-free laser diode with high feedback tolerance has driven extensive global research, yet no "Holy Grail" solution has emerged to date.

To overcome the drawbacks inherent to DFB lasers, we considered using non-Hermitian, complex-coupled BGs, combining modulation of the real and imaginary parts of the waveguide's effective index with a controlled phase shift between them. The index-modulated grating ensures there is a lower threshold injection current, while the presence of losses enhances the laser mode discrimination mechanism and improves the robustness of single-frequency operation [10,11]. Furthermore, theoretical studies suggest that the unidirectional reflection characteristic of a Parity-Time symmetric BG [12], corresponding to a quarter-period phase shift between the real and imaginary parts of the effective index, should make the laser more robust against in-line optical feedback [12]. Ideally, no optical isolators would be required, which should significantly reduce the component's cost.

The objective of this work was to conduct a lasing-oriented comparative modeling study of the main types of complex-coupled DFB (CC-DFB) lasers, sampling the main types that were considered in [10,13], with particular emphasis on the symmetry aspects of the complex-index-profile BG; that is, how gain and losses are modulated along the direction of light propagation. Notably, ref. [13] is generic, and another previous study [10] was more narrowly focused on conventional DFB lasers with dielectric BGs, DFB lasers with metallic gratings, and complex-coupled DFB lasers featuring phase-shifted dielectric and metallic gratings with limited parametric scan capacity.

The aim was to find the optimal design of DFB lasers in terms of spectral behavior, the threshold gain level, and the modal gain contrast between the lowest-gain pole and the next higher pole. This involved addressing the question of the optimal amplitude of modulation of the real and imaginary parts of the complex index profile and that of the optimal phase shift between the real and imaginary modulation of the index profile, along with the impact of the arbitrary termination of facets, an aspect that is difficult to control in practice.

Before diving into the details, we note that a more general physical view of lasing non-Hermitian systems has recently been proposed by Akhter et al. [14,15]. In the case of a manifold of propagating modes all propagating in the same direction, a periodic modulation with PT-symmetry can scatter modes with a unidirectional character (mode A scatters into B, but not vice versa). These papers propose a clever way to exploit this class of phenomena to achieve "mode cleaning", which is clearly of interest in regard to broad waveguides (fibers, power lasers, etc.). While these concepts do not directly address ours, we note that in a recent contribution [16], the authors proposed yet another different approach to the scattering of PT-symmetric systems depending on the presence of "looped" feedback, which leads to interesting and elegant "normal forms" of coupling physics. However, it is currently unclear whether these "looped" forms of feedback act the same way as the traditional DFB feedback. Interferences do not fabricate nodes and antinodes in the same way, but a change of perspective may reconcile these views, possibly helping to encapsulate the physics of CC-DFB, which we consider here in a broader unified framework—a commendable aim per se. At the present stage, we prefer to present our work in a way that privileges its connection with previous experimental and theoretical results regarding DFB lasers that are sufficiently similar, without yet resorting to the broader non-Hermitian framework.

This article is organized as follows. The optimal design of first-order CC-DFB lasers without facet coatings is addressed in the next section. Section 3 is dedicated to highlighting the potential of Parity-Time symmetry for DFB laser applications. Section 4 concludes the article with a summary and an outlook.

2. Optimal Design of First-Order CC-DFB Lasers Without Facet Coatings

2.1. CC-DFB Laser Modeling Approach

Figure 1a illustrates the principle of a CC-DFB laser with a BG made up of physically separate components for modulating the real and imaginary parts of the effective index, observed as two (complex) additive contributions by the lasing mode of the ridge waveguide. The experimental realization of CC-DFB lasers exploiting such a grating architecture was reported in the context of our recent demonstration of light-by-light manipulation of laser emission via a tunable ultra-short external cavity [14].

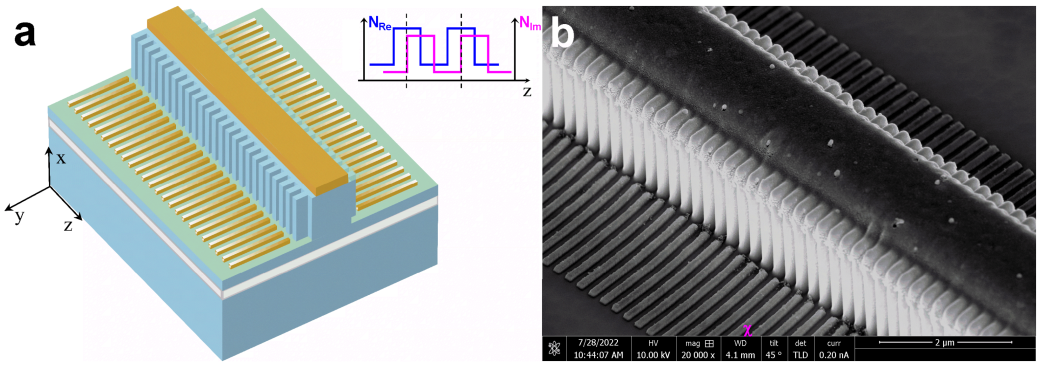


Figure 1. (**a**) Rendering of the C-C DFB laser. Blue (dielectric) and yellow (metallic) gratings are shown. The inset depicts the complex effective index profile. (**b**) SEM perspective view of the fabricated first-order C-C DFB laser.

The real part of the refractive index is modulated by varying the width of the waveguide ridge, while the imaginary part of the index is modulated using a metallic BG positioned on either side of the ridge waveguide. The experimentally realized complex-coupled Bragg-grating-assisted waveguide structure is shown in Figure 1b. On the basis of experimental and modeling studies reported in [11] for a similar complex-coupled BG structure—albeit operating at the third order rather than the first, as in our case—the modulation amplitudes of the real and imaginary parts of the grating's refractive index profile are $\Delta n_{\mathrm{Re}} = 0.002$ and $\Delta n_{\mathrm{Im}} = 0.0004$, respectively. As shown later, this choice, where $\Delta n_{\mathrm{Im}} << \Delta n_{\mathrm{Re}}$, represents a good compromise between fabrication constraints and the requirement for operation with a sufficiently low threshold gain.

We thus operate relatively far from a PT-symmetric point, in the broken region, with the addition of the "continuous background" active layer still playing a large role in the attainment of the threshold. We do not capitalize on specific features of the Exceptional Points, but unidirectionality does have an effect, as shown in some specific results.

To determine the optimal design of CC-DFB lasers, we consider an Abelès transmission matrix method model of a Bragg mirror structure with a complex refractive index profile (shown schematically in Figure 2). In this model, each period Λ is divided into eight layers of thickness $\Lambda/8$. The spatial phase shift Ψ between the rising edges of the modulations in the real and imaginary parts of the refractive index corresponds to an integer multiple m of $\pi/8$ (i.e., m $\times$ 45°). The real part of the index profile is set to $n_{\mathrm{Re+}} = n_{\mathrm{eff_WG}} + \Delta n_{\mathrm{Re}}/2$ over a half-period $\Lambda/2$ and $n_{\mathrm{Re-}} = n_{\mathrm{eff_WG}} - \Delta n_{\mathrm{Re}}/2$ over the subsequent half-period. In this case, for laser emission polarization TE, the mean effective index of the waveguide obtained via modeling and deduced from experimental data is as follows: $n_{\mathrm{eff_WG}} \approx 3.23$ [11].

Similarly, the imaginary part is $n_{\mathrm{Im-}} = -ig + i\Delta n_{\mathrm{Im}}$ over one half-period and $n_{\mathrm{Im+}} = -ig$ over the next half-period, where g represents the variation in the imaginary part of the refractive index induced by the introduction of gain into the structure. For instance, an imaginary refractive index component of $i = 10^{-4}$ at a wavelength of 1.55 µm corresponds to a gain level of G = 35.21 dB/cm.

The threshold gain level can be determined by modeling the DFB laser array with such a 1D periodic stack of layers with a thickness of $\Lambda/8$ whose refractive index matches the effective index of the Bragg waveguide at the corresponding position along the light propagation axis, as shown in Figure 3. The facets' termination is accounted for by adding left and right zones with an incomplete period (the outside medium is air or a vacuum, with a refractive index $n = 1$; hence, there is significant reflectivity amounting to about 28%). The length of these zones may be arbitrary and is not bounded by the condition that it must be an integer number of $\Lambda/8$. For convenience, the ratio $L_{\mathrm{facet}}/\Lambda$ is denoted as Φ_{in} and Φ_{out} for the input and output facets, respectively.

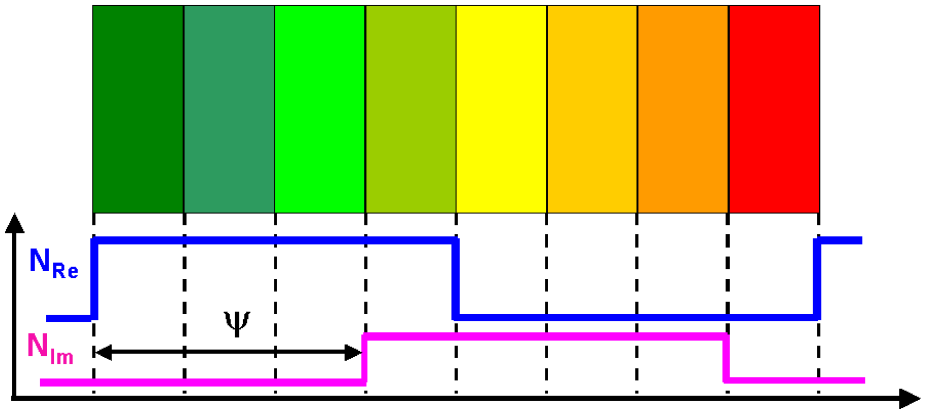


Figure 2. Schematic of the complex index profile BG period modeled via the Abelès transmission matrix method. Each period Λ is composed of equal thickness Λ/8 layers with complex refractive index values n_{Re} and n_{Im}. The phase shift Ψ between real and imaginary refractive index modulation is equal to an integer number m of π/4 (i.e., m × 45°).

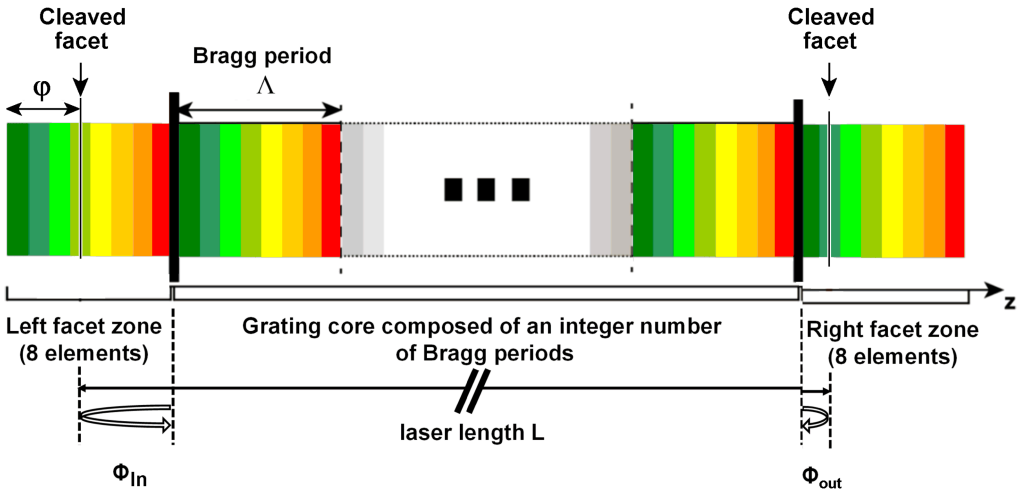


Figure 3. Schematic of the BG with a complex index profile modeled using the transfer matrix method. The phases Φ_j of the two facets (eventually with AR and HR coatings) are swept throughout the 1-period-long outer zones. This period is much smaller than the total length (Λ << L). The phase φ represents the shift in the BG's refractive index modulation period relative to the input facet.

2.2. First-Order Dielectric Grating DFB Laser

For a rectangular grating profile, the relation between the BG coupling coefficient c and the waveguide effective index modulation Δn_{Re} is as follows:

$$\chi = \frac{\Delta n_{RE}}{\Lambda n_{RE}} \quad (1)$$

Given that Λ = 0.24 μm, n_{Re} = 3.228, and Δn_{Re} = 0.002, χ = 2.58 × 10^{-3} μm^{-1}. Thus, for an L = 1 mm long grating, the coupling strength χL = 2.58, which is sufficient for laser operation. Consequently, the modulation of the real part of the refractive index Δn_{Re} = 0.002 is only considered in the rest of this study.

Figure 4a shows the distribution as a function of wavelength of the transmission poles for a 1 mm long conventional DFB laser with modulation of only the real part of the refractive index. This modeling was performed for one of the two optimal configurations of facet termination in terms of the lowest threshold gain (shown in Figure 4c) with Φ_{in} = 311° and Φ_{out} = 134°. In this case, the lowest pole at G_{th} = 18 dB/cm corresponds to the onset of laser emission for a wavelength below the BG bandgap centered around 1.549 μm. The

gain level contrast with respect to the second-lowest pole located at a wavelength above the BG bandgap is 12 dB/cm.

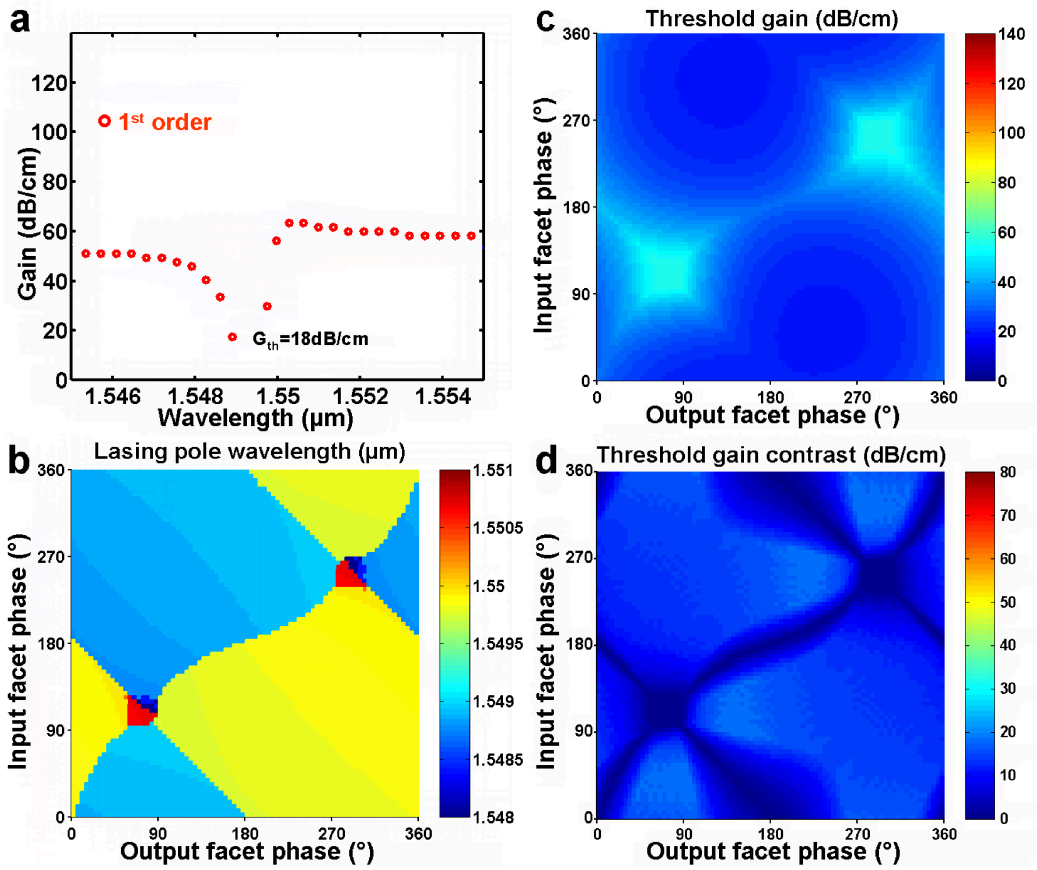


Figure 4. (**a**) Map of the position of the transmission matrix poles for a 1st-order 1 mm long dielectric BG with refractive index modulation $\Delta n_{Re} = 0.002$. (**b**) Color map showing variation in the emission wavelength at the threshold gain level as a function of input and output facet termination. (**c**) Color map showing variation in the threshold gain level as a function of input and output facet termination. (**d**) Color map showing variation in the threshold gain contrast between the lowest pole and the immediately higher one as a function of input and output facet termination.

Figure 4b presents a color map showing the emission wavelengths for the poles with the lowest gain as a function of facet variation. As shown, the blue region, mainly located in the upper-left corner of the map, corresponds to wavelength emission below the bandgap (the higher-frequency edge of the bandgap). The yellow region, located essentially in the lower-right corner of the map, corresponds to wavelength emission above the bandgap (the lower-frequency edge of the bandgap). Operation near the border of the blue and yellow regions corresponds to dual-wavelength operation, which obviously does not meet telecommunication requirements.

The color map in Figure 4c shows the variation in the threshold gain level as a function of the input and output facet terminations. Figure 4d provides a color map showing the variation in the threshold gain contrast between the lowest pole and the second highest one as a function of input and output facet termination. Evidently, although the gain at the threshold is low, the gain contrast relative to the immediately higher pole is also low.

Such a gain contrast cannot guarantee robust single-frequency laser emission. Owing to the inhomogeneous linewidth broadening characteristic to semiconductor lasers, increasing the gain level with injection current results in the onset of lasing for higher-gain-level poles. This explains the multi-wavelength laser emission observed experimentally for the third-order DFB lasers reported in [11].

Note that the poles located far from the bandgap at G_{th_FP} = 56 dB/cm are those of the Fabry–Perot (FP) cavity; i.e., the wave essentially averaging all grating effects, formed by the end facets with 28% reflection.

As the dielectric BG is one of the two components of complexly coupled DFB lasers, it is important to acquire insight into the origin of the observed evolutions of gain threshold and spectral response with facet variation. Accordingly, it is necessary to separate the contribution due to the variation in cavity length from that related to the phase shift $\varphi = 2\pi - \Phi_{in}$ of the modulation of the BG refractive index profile with respect to the input end of the grating (Figure 3).

To perform such an analysis, four DFB cavity lengths corresponding to an integer number of periods N as well as a fractional number of periods N + 0.25, N + 0.5, and N + 0.75 are considered. For each DFB cavity length, we study eight types of configurations corresponding to the phase shift φ by steps of 45° (Λ/8). All 32 possible configurations examined are shown in Figure 5a.

Note that for each cavity length considered, only five configurations out of eight related to φ phase shift variation are genuinely dissimilar. The counterparts of the other three correspond to an inversion symmetry relationship, as illustrated in Figure 5b. To gain more insight into the impact of phase shift φ with respect to facet termination, a map of the position of the transmission matrix poles for different DFB cavity lengths is presented in Figure 6.

The spectral distribution of the transmission matrix lasing poles for a DFB cavity with a length of about 1 mm with an integer number of periods N = 4167 is shown in Figure 6a. As shown, when φ = 0° or 180°, the spectral distribution is symmetrical with respect to the position of the Bragg wavelength λ_{Br} = 1.5494 μm, corresponding to the middle of the bandgap. The lowest poles are at the edges of the bandgap, resulting in dual-wavelength laser operation. These phase shifts of φ = 0° or 180° correspond to the situation where the grating begins and ends with a complete half-period of a higher or lower refractive index, respectively. This is the most common BG configuration conventionally studied in the literature [13].

However, the spectral distribution becomes strongly asymmetrical for other phase shifts, notably when φ = 90° or 270°, even though these gratings' refractive index profiles exhibit both mirror and inversion symmetry. For instance, the configuration with φ = 90° corresponds to the situation where the BG begins and ends with a quarter period of a higher refractive index: $n_{Re+} = n_{eff_WG} + \Delta n_{Re}/2$. The lowest pole is located at the short-wavelength edge of the bandgap. For the configuration where φ = 270°, the grating begins and ends with a quarter period of a lower refractive index: $n_{Re-} = n_{eff_WG} - \Delta n_{Re}/2$. The lowest pole is now located at the long-wavelength edge of the bandgap.

The physical mechanism behind these results is related to the interaction of two resonance phenomena present in a DFB cavity. The first is associated with Fabry–Pérot (FP)-type resonances which, in the absence of a grating, lead to mode selection corresponding to an integer number of half-wavelengths over the length of the optical cavity. The second arises from mode selection induced by the resonant properties of the BG. The poles of the transmission matrix for the "bare" FP cavity, the "bare" BG without reflection from facets, and the DFB confined by a FP cavity with BG, where φ = 0° of lengths N and N + 0.5 periods, are represented in Figure 7a,b.

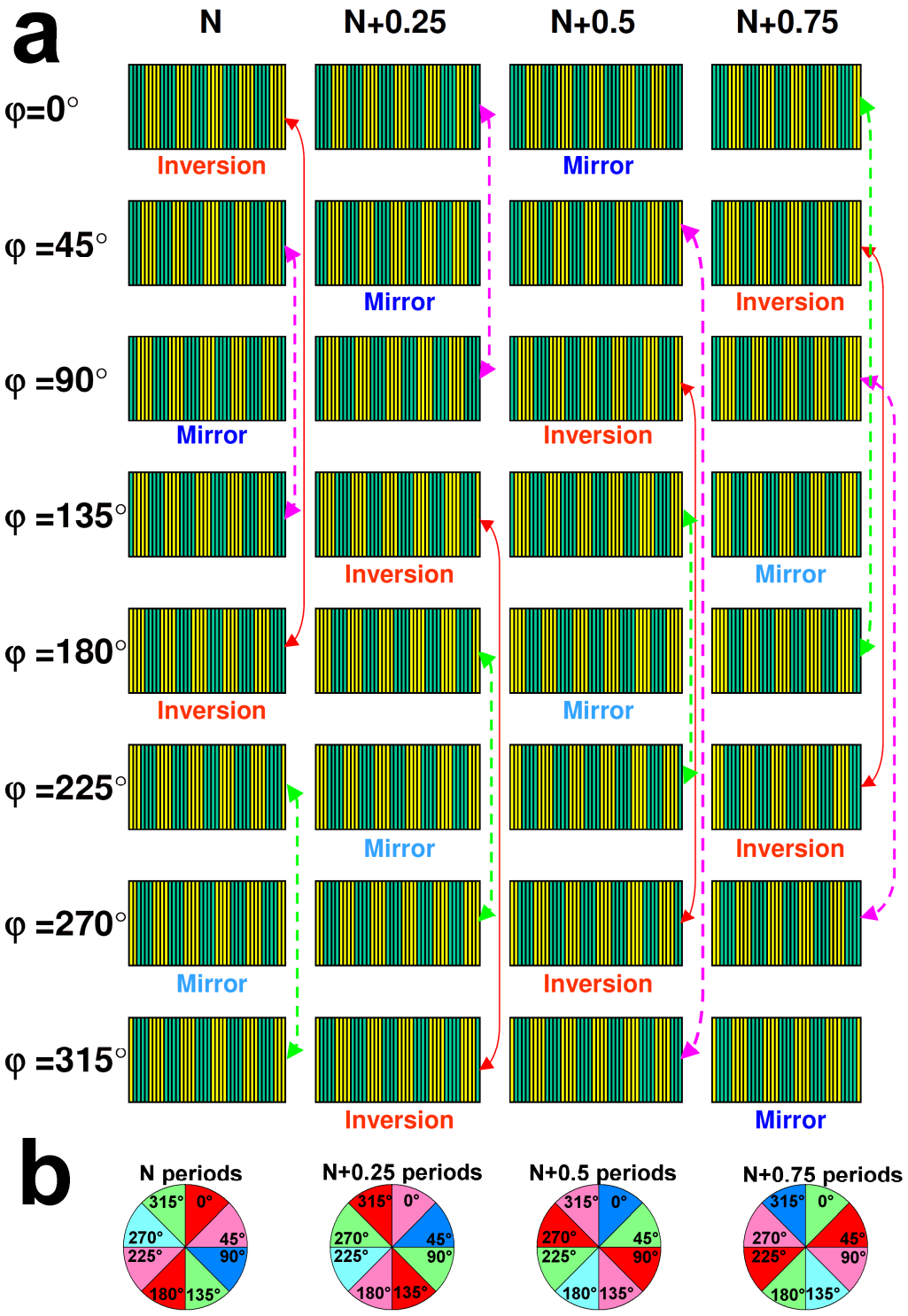


Figure 5. (**a**) Schematic of various dielectric grating configurations corresponding to an integer number of periods N, as well as fractional numbers of periods N + 0.25, N + 0.5, and N + 0.75, as a function of the phase shift φ varying in 45° increments. Green indicates grating sections with $\Delta n_{\mathrm{Re}} = +0.001$, and yellow indicates those with $\Delta n_{\mathrm{Re}} = -0.001$. Note that the surrounding medium is air ($n = 1$). Curves marked with red arrows indicate identical configurations possessing intrinsic inversion symmetry, while curves marked with magenta and green arrows indicate identical configurations lacking specific intrinsic symmetry. (**b**) Mnemonic representation of the evolution of grating symmetry as a function of the variation in the fractional number of periods. Sector color codes: Red for inversion symmetry; dark and light blue for mirror symmetries; and green and magenta for identical configurations lacking specific intrinsic symmetry.

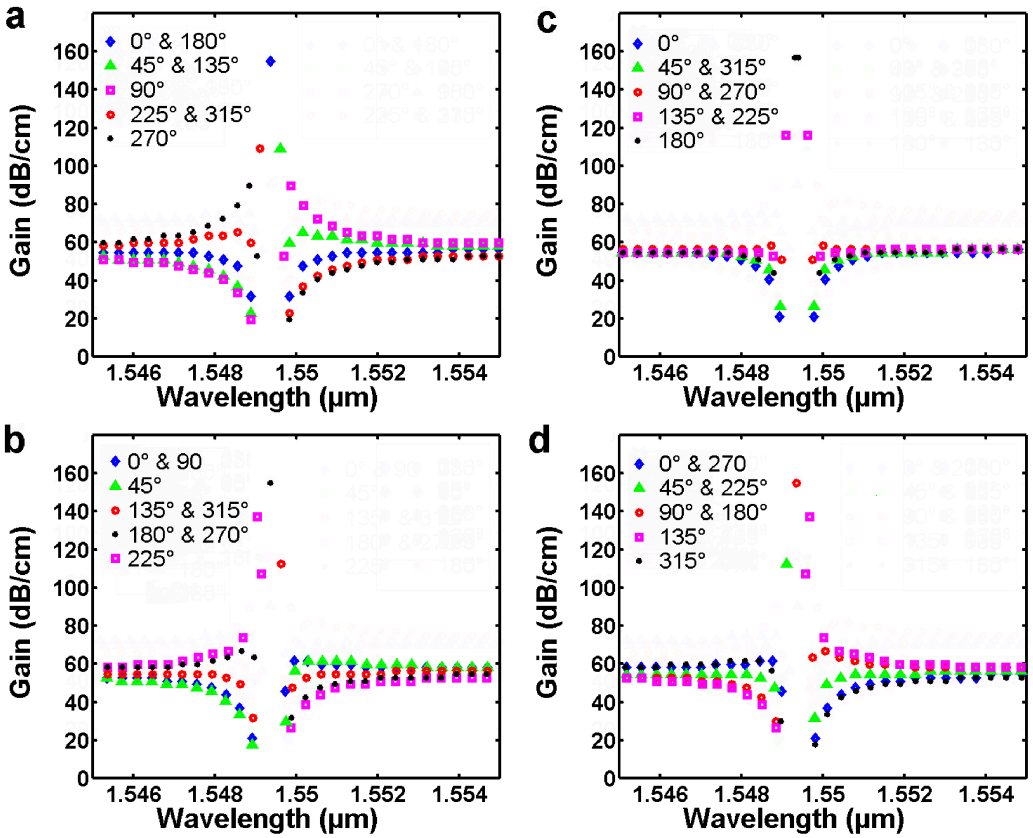


Figure 6. Map of the position of the transmission matrix poles for a 1st-order, 1 mm long dielectric BG as a function of refractive index profile modulation phase shift φ with respect to the input facet. DFB cavity length: (**a**) N periods; (**b**) N + 0.25 periods; (**c**) N + 0. 5 periods; and (**d**) N + 0.75 periods.

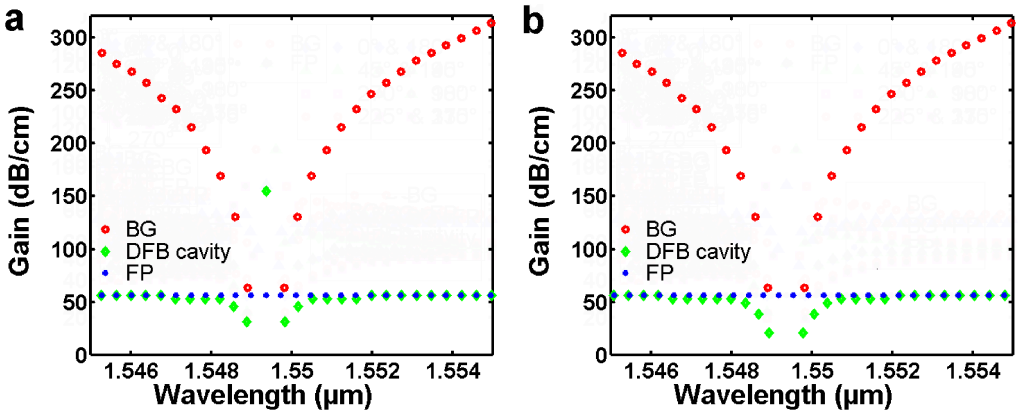


Figure 7. Map of the position of the transmission matrix poles for a 1 mm long bare FP cavity, a bare Bragg grating without end reflection, and a 1st-order DFB cavity with φ = 0°. (**a**) N-period-length structure. (**b**) N + 0.5-period-length structure.

Evidently, for an N-period-length BG structure, there are three poles of the bare FP cavity, which are located in the bandgap spectral interval of the bare BG. The Nth pole of the FP cavity is located exactly at λ_{Br}. The spectral positions of the poles of the FP cavity Nth − 1 and Nth + 1 are very close to those located at the edges of the bandgap of either the bare BG or the DFB cavity with a phase shift of φ = 0° or 180°. More generally, outside the immediate vicinity of the bandgap, the spectral positions of the poles of the bare BG, the bare FP, and DFB cavities almost coincide, implying that strong interaction between the two resonance mechanisms, induced by the BG and FP cavity, respectively, occurs only in the immediate vicinity of the bandgap.

Note that the Nth pole of the DFB cavity is also located in the middle of the bandgap, but its gain level is much higher than the levels of the rest of the poles of the DFB cavity owing to the strong attenuation of light transmission in the bandgap. In practice, such a pole will never attain lasing, and it will remain dark. This dark pole, absent in the case of a bare BG, is that of an FP cavity. Its particularity is that the spatial periodicity of the variation in light intensity along the cavity at λ_{Br} coincides with that of the refractive index profile of the BG. The interfaces between a high refractive index (nH) and a lower refractive index (nL) in this case are located either at a node or an antinode of light intensity distribution. This assertion is fully supported by the results regarding the calculated electric field distribution, which are presented in Figure 3a of Ref. [13] for a similar type of BG with an integer number of periods.

The situation changes with the introduction of the phase shift φ between the modulation of the refractive index profile and the facets of the DFB cavity. The mirror symmetry of the spatial positions of the nH/nL and nL/nH interfaces where the reflection occurs is lost. As a result, the standing wave pattern formed by the interaction of reflections from the cavity mirrors and those caused by the grating is modified. The spectral position of the dark-mode shifts toward the higher-wavelength edge of the bandgap. At the same time, the threshold gain level of the poles below the bandgap lowers, while that of the poles above the bandgap increases. Single-frequency laser operation can occur in this case, corresponding to the lowest pole at the short-wavelength edge of the bandgap. The maximum asymmetry favoring single-frequency emission is reached around $\varphi = 90^\circ$ when the DFB cavity ends with quarter-period nH layers.

An opposite situation occurs when $\varphi = 270^\circ$. This time, the DFB cavity ends with quarter-period nL layers. Although, at first glance, the two configurations appear quite similar, the spatial distributions of the reflected phases are different because of the inverted arrangement of the nL/nH interfaces. This point is important since there is an additional π phase shift when light incident from the nL layer is reflected from the interface with the nH layer. Consequently, the asymmetry of the spectral distribution of the poles of the transmission matrix is opposite relative to the configuration with $\varphi = 90^\circ$. Single-frequency laser operation can occur in this case at the long-wavelength edge of the bandgap. Note that the distribution along the grating of nL/nH and nH/nL interfaces for this case is inverse with respect to that of the $\varphi = 270^\circ$ configuration.

It is instructive to compare these results with those of the DFB cavity with a length of N + 0.5 periods shown in Figure 6c. This time, the spectral distribution of the poles of the transmission matrix is symmetrical with respect to λ_{Br} for the different φ phase shifts considered. The difference from the N-period-length structure is that, as shown in Figure 7b, there are only two poles of the bare FP cavity located within the bandgap spectral interval of the bare BG. The spectral positions λ_N and λ_{N+1} of these FP cavity poles are symmetrical with respect to λ_{Br}. Therefore, the spatial periodicity of the variation in light intensity along the cavity at the wavelengths of these poles does not correspond to the refractive index profile of the BG. Since $\lambda_{N+1} < \lambda_{Br}$ while $\lambda_N > \lambda_{Br}$, the periodicity mismatch at these two wavelengths is of the opposite sign. The φ phase variation via the mechanism detailed above leads to a shift in the wavelength of the Nth and Nth + 1 poles either towards the edges of the bandgap and a lower threshold gain level when $\varphi = 0^\circ$ (nH external layers of half-period) or towards the middle of the band gap with dark-mode behavior when $\varphi = 180^\circ$ (the external layers of the half-period nL).

Evidently, for a DFB cavity with an intermediate length of N + 0.75 and N + 0.25 periods, the spectral positions of the FP poles that lie within the bandgap of the bare BG are not symmetrical with respect to λ_{Br}. Therefore, the spectral distribution of the transmission matrix poles is asymmetric, resulting in laser operation either at short- or long-wavelength

edges of the bandgap. The poles' spectral distributions for a DFB cavity with N + 0.75 and N + 0.25-period lengths are shown in Figures 6d and 6b, respectively. The threshold gain levels of the $\varphi = 315^\circ$ pole for the N + 0.75-period grating and the $\varphi = 45^\circ$ pole for the N + 0.25-period grating are even somewhat lower relative to the lowest poles of the N− and N + 0.5-period BGs.

It is these very configurations that are very close to the two lowest threshold gain facet termination levels shown in Figure 4c. The first one, with $\Phi_{in} = 311^\circ$ and $\Phi_{out} = 134^\circ$ when laser emission occurs at the short-wavelength edge of the bandgap, corresponds approximately to that shown in Figure 5 for a grating length of N + 0.25 periods, where $\varphi = 45^\circ$. In this case, the grating begins and ends with $3\Lambda/8$ nH layers. The second one, with $\Phi_{in} = 56^\circ$ and $\Phi_{out} = 232^\circ$ when laser emission occurs at the long-wavelength edge of the bandgap, corresponds approximately to that for the grating length of N + 0.75 periods, where $\varphi = 315^\circ$. In this case, the grating begins and ends with $\Lambda/8$ nL layers. The common feature of these two configurations is that, in both cases, the grating exhibits mirror symmetry. This assertion is fully supported by the results regarding the calculated electric field distribution, which are presented in Figure 3a of Ref. [13] for a similar type of BG with an integer number of periods.

In summary, although single-frequency operation of dielectric-grating DFB lasers is possible in principle, their use in practical applications presents two major drawbacks. The first stems from the inability to control the position of the wavelength of laser emission, which can occur either below or above the bandgap depending on the length of the cavity and the arbitrary facet termination phase. The second drawback lies in the relatively low gain contrast between the lowest-gain pole and the second lowest one, leading to multi-wavelength laser emission once the gain reaches a sufficiently high level. Furthermore, when the length of the cavity is close to N + 0.5 periods, dual-wavelength laser emission is generally expected, regardless of the facet termination phase.

The conventional solution to the single-wavelength operation problem involves using a quarter-wave-shifted BG. This entails introducing a $\lambda/2$-type defect at the center of a BG, acting as a phase shifter and AR-coated facets. Another solution, based on a similar principle but employing a different mechanism, is proposed in the following section. However, as we shall see, none of these solutions resolves the issue of the relatively low gain contrast between the DFB cavity modes. Consequently, alternative solutions based on a mode selection mechanism that exploits wavelength-selective absorption are considered below.

2.3. First-Order Metallic Grating DFB Laser

The mechanism for selecting the emission wavelength for a metallic DFB laser is radically different relative to that for a dielectric DFB laser. It primarily depends on the distribution of the electromagnetic field (in the form of a standing wave) within the laser cavity relative to the absorbing metallic elements of the BG. The configuration most favorable for laser emission is one in which the electromagnetic field maxima maximally avoid all the regions of metallic absorption. This optimal condition is achieved when the length of the DFB cavity corresponds to an integer number of periods and the facet phases $\Phi_{in} = 270^\circ$ and $\Phi_{out} = 90^\circ$. As illustrated in Figure 8a, this situation corresponds to the case where the BG begins and ends with a metal-free section with a length equal to one-quarter of the period. This assertion is also supported by the results regarding the calculated electric field distribution, which are presented in Figure 3b of Ref. [13] for a similar type of BG featuring modulation of the imaginary part of the refractive index profile.

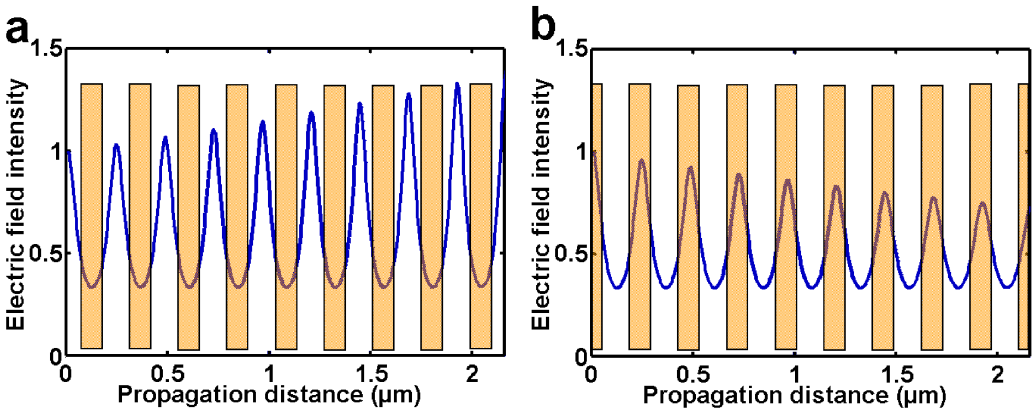


Figure 8. Electromagnetic field intensity distribution along the direction of light propagation from left to right at the Bragg wavelength. The average gain level is equal to the average loss level along the BG. The metal absorption region is given in orange. (**a**) $\Phi_{in} = 270°$, and $\Phi_{out} = 90°$; (**b**) $\Phi_{in} = 90°$, and $\Phi_{out} = 270°$. Note the distinct behaviors as the standing wave component preferably samples the lossless or the lossy regions.

In the specific example shown in Figure 8a, the average gain was set such that it was equal to the average loss along the BG. However, evidently, the light intensity propagating in the BG from left to right grows with the propagation distance, as the standing wave component preferably samples the white lossless regions. The opposite occurs when we consider the BG represented in Figure 8b, which begins and ends with a metallic section with a length equal to one-quarter of the period of the BG. Here, the light intensity propagating in the BG from left to right decreases with an increase in propagation distance. The configuration illustrated in Figure 8b, where $\Phi_{in} = 90°$ and $\Phi_{out} = 270°$, corresponds to the worst condition (antinodes in metal) with the highest threshold gain.

Figure 9a presents the distribution as a function of wavelength of the transmission poles for a first-order 1 mm long metallic grating DFB laser featuring modulation of only the imaginary part of the refractive index $\Delta n_{Im} = 0.0004$. This modeling was performed for the optimal facet termination in terms of the lowest threshold gain considered above. In this case, the onset of laser emission at the lowest pole with $G_{th} = 77$dB/cm occurs at λ_{Br}. The distributions of the threshold gain for the lowest-gain mode and of the gain contrast relative to the next-highest-gain mode are shown in Figures 9c and 9d, respectively. The gain level contrast at λ_{Br} with respect to the next lowest poles is ~48 dB/cm. This gain contrast is four times higher than that of the dielectric grating DFB laser of the same length. This is due to the increase in the threshold gain of the Fabry–Pérot cavity poles caused by the non-resonant absorption of the metallic grating. This explains the 50 dB high side mode suppression ratio (SMSR) level observed experimentally for the first-order metallic grating DFB lasers reported in [11].

Furthermore, as shown in Figure 9b, the emission wavelength generally depends little on facet termination. The variation in emission wavelength corresponding to the region outlined in yellow (characterized by lower threshold gain (see Figure 9c)) is on the order of a few tenths of nanometers, representing a fraction of the free spectral range (FSR) of the Fabry–Pérot cavity. However, the improvement in single-longitudinal-mode operation comes at the cost of a threshold gain level approximately four times higher than that of DFB lasers with dielectric gratings. It therefore appears that neither DFB lasers with dielectric gratings nor those with metallic gratings constitute entirely satisfactory solutions. Nevertheless, as shown in Section S1 of Supplementary Material (SM), the modulation of the imaginary part of the refractive index $\Delta n_{Im} = 0.0004$ used in the current modeling represents a satisfactory compromise between the threshold gain level and the gain contrast

between the lowest energy mode and the FP cavity mode. This value was therefore adopted for the further study of complex-coupled DFB lasers (assuming that fine tuning yields improvements only at the next expansion order of the modulation perturbation).

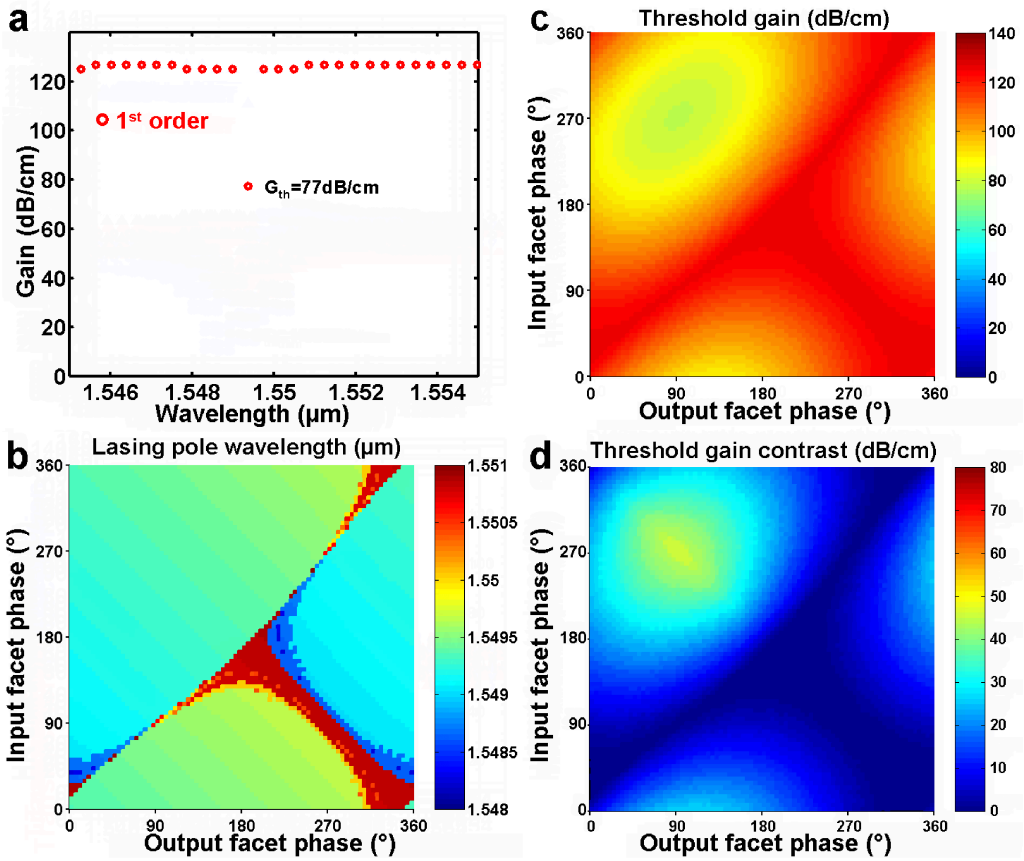


Figure 9. (**a**) Map of the position of the transmission matrix poles for a 1st-order 1 mm long metallic BG featuring refractive index modulation $\Delta n_{\mathrm{Im}} = 0.0004$. (**b**) Color map showing the variation in the emission wavelength at the threshold gain level as a function of input and output facet termination. (**c**) Color map showing the variation in the threshold gain level as a function of input and output facet termination. (**d**) Color map showing the variation in the threshold gain contrast between the lowest pole and the immediately higher one as a function of input and output facet termination.

2.4. First-Order CC-DFB Lasers (Ψ = 0° or Ψ = 180°)

To study the behavior of the CC-DFB lasers, we consider a special case characterized by high symmetry in the grating's refractive index profile, where the modulation of real ($\Delta n_{\mathrm{Re}} = 0.002$) and imaginary ($\Delta n_{\mathrm{Im}} = 0.0004$) parts is either in-phase ($\Psi = 0°$) or in antiphase ($\Psi = 180°$). To better understand the behavior of these lasers, it is instructive to first examine the properties of bare complex-coupled BGs without end reflections. The distribution of transmission poles as a function of wavelength for this situation is illustrated in Figure 10a. Evidently, for $\Psi = 0°$, the pole with the lowest gain is located at the long-wavelength edge of the bandgap, whereas for $\Psi = 180°$, it lies at the short-wavelength edge of the same bandgap.

Similar behavior can also be observed in the presence of facet reflectivity. The distribution as a function of wavelength of the transmission poles of such a first-order 1 mm long CC-DFB laser where $\Psi = 0°$ is shown in Figure 11a. This modeling was performed for the optimal configuration of facet termination in terms of the lowest threshold gain shown in Figure 11c, with $\Phi_{\mathrm{in}} = 0°$ and $\Phi_{\mathrm{out}} = 180°$. This configuration corresponds to the case where the BG begins and ends with a complete half-period corresponding to a higher index nH and a metal-free region. In this case, as represented in Figure 11b, the onset of

laser emission at the lowest pole with Gth = 53 dB/cm occurs at the long-wavelength edge of the bandgap. This finding is perfectly consistent with the transmission and reflection modeling results shown in Figure 4a of Ref. [13] for a similar type of complex-coupled BG with an integer number of periods.

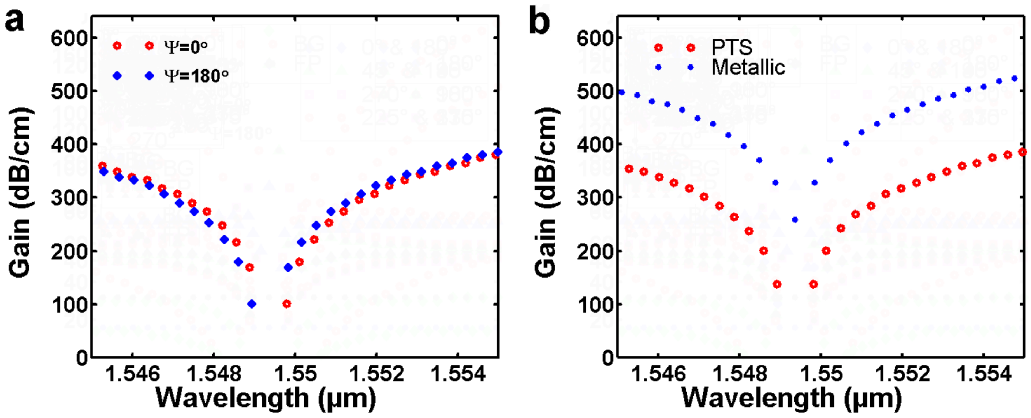


Figure 10. Map of the position of the transmission matrix poles for a 1st-order ~1 mm N-period structure. (**a**) Bare complex-coupled BGs (Ψ = 0° and Ψ = 180°) without end reflection (see Section 2.4). (**b**) Bare PT-symmetric and metallic BG without end reflection (see Section 2.5).

Moreover, the blue-green region delimited by the yellow boundary in Figure 11c, which corresponds to the lower threshold gain, represents approximately 80% of the area of the color map, while the less favorable red one constitutes only 20%. This should be compared to the coverage of about 40% of the area of the color map corresponding to a similar gain level in the case of a metallic grating DFB laser, as shown in Figure 9c. This feature would result in a much higher fabrication yield of lasers with suitable performance, one comparable or better than that of state-of-the-art mass-produced laser diodes. A similar situation can be observed regarding the gain contrast illustrated in Figures 9d and 11d.

Furthermore, the distribution of the threshold gain favorable for lasing in the CC-DFB, delimited by the yellow boundary, is much flatter than that of the DFB laser with a metallic grating shown in Figure 9c. The same applies for the gain contrast illustrated in Figures 9d and 11d. Lastly, for the metallic case, the lowest threshold gain unfortunately coincides with the largest differential threshold gain, a trend that concerns only a minority of the map area for the CC-DFB case, which mostly features low threshold gain together with low differential threshold gain.

Consequently, the CC-DFB laser can be expected to be much more robust in terms of single-mode lasing than its metal-grating counterpart. This hypothesis was experimentally verified in our recent publication [17], where a high-reflectivity gold micromirror was placed in very close proximity (on the order of a few wavelengths) to the cleaved facet of a DFB laser to simulate the phase variation induced by arbitrary facet termination. The main result was that, above the threshold, the metal-grating DFB laser exhibited unstable single-frequency emission, accompanied by significant linewidth broadening, typical of a coherence collapse. In contrast, the CC-DFB laser maintained robust single-frequency operation.

Notably, such DFB lasers, coupled with a tunable external cavity, have been used in a previously unexplored regime featuring ultra-strong coherent optical feedback, where nearly 90% of the emitted optical field is reinjected into the DFB laser. The feedback mechanism—involving a phase shift induced by the mirror of the tunable external cavity, which is itself actuated by a piezoelectric stage—is basically similar to that of conventional external optical feedback. However, in our case, the feedback power level is at least two

orders of magnitude higher, and the interference effects accompanying laser emission are far more pronounced since light coherence is preserved. Lastly, the lifetime of photons is not very long in our proposed AR/HR lasers because of the AR side. Thus, large-delay coherent feedback hardly impacts the condition of such lasers, whose own "memory" is limited.

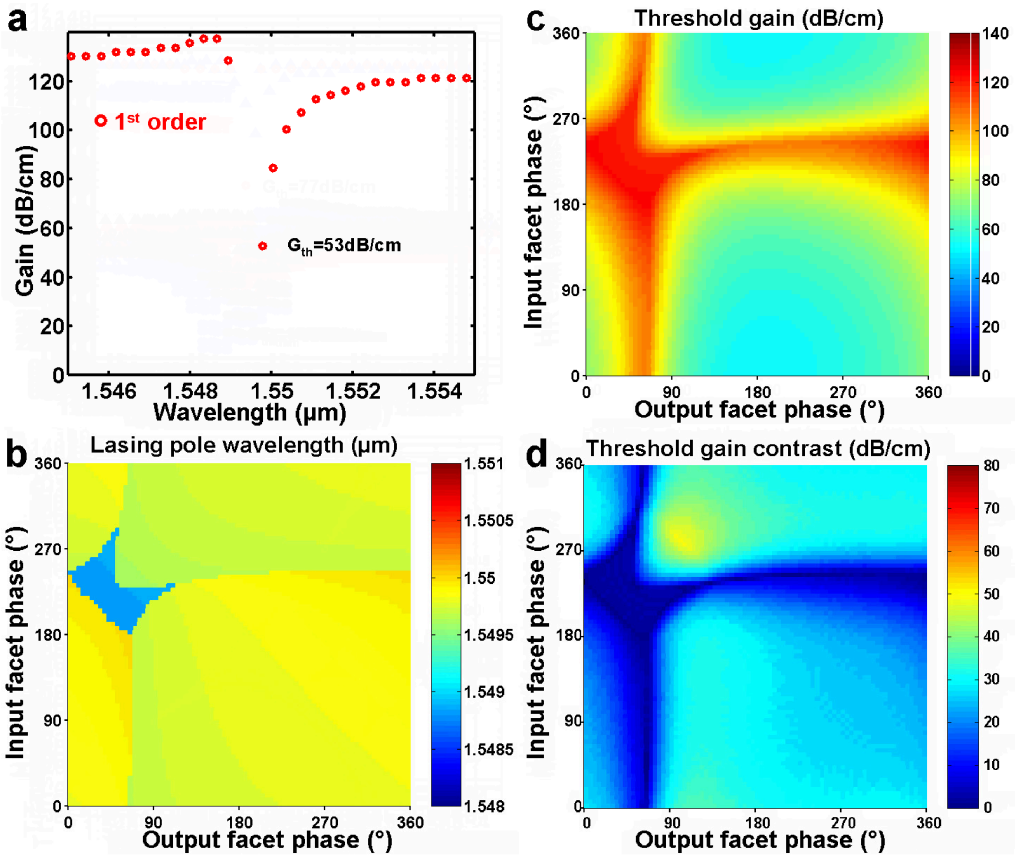


Figure 11. (**a**) Map of the position of the transmission matrix poles for a 1st-order 1 mm long complex index profile BG with $\Psi = 0°$ and refractive index modulation $\Delta n_{Re} = 0.002$ and $\Delta n_{Im} = 0.0004$. (**b**) Color map showing variation in the emission wavelength at the threshold gain level as a function of input and output facet termination. (**c**) Color map showing variation in the threshold gain level as a function of input and output facet termination. (**d**) Color map showing variation in the threshold gain contrast between the lowest pole and the immediately higher one as a function of input and output facet termination.

In light of these considerations, one can reasonably expect stable single-frequency operation of CC-DFB lasers in this regime consisting of ultra-strong coherent optical feedback to exhibit greater robustness than conventional optical feedback, which is of low intensity and not necessarily coherent, thereby introducing the prospect of potentially isolator-free operation, although further experimental studies are still required to verify this hypothesis.

Finally, an additional major improvement lies in the fact that the CC-DFB laser exhibits high emission wavelength stability. This can be directly inferred from the data presented in Figure 11b. This characteristic is explained by the fact that the interaction between the dielectric grating's resonance phenomena and the absorption induced by the metal grating fixes, by design, the emission wavelength corresponding to the lowest gain threshold. Thus, the CC-DFB laser combines the advantages of the metal-grating DFB laser (high gain contrast, with stable single-mode emission) with those of the dielectric DFB laser (a lower gain threshold and higher efficiency), making it attractive for practical applications. This also explains the markedly superior performance of third-order CC-DFB lasers relative to

either the third-order dielectric-grating DFB lasers or first-order metal-grating DFB lasers reported in [11].

Experimental observations revealing the facet termination phase's large influence on the threshold gain and emission power of first-order metal-grating lasers and CC-DFB lasers (with $\Psi = 0°$) were reported in our recent publication [17]. The experimental results and the significant threshold modulation that they display relative to the phase of the mirror feedback (providing overall reflectivity of more than an equivalent facet for distances of a few wavelengths) are consistent with modeling predictions.

Note that the case where the dielectric and metallic gratings are in antiphase ($\Psi = 180°$) yields similar results, except that the emission now occurs at the short-wavelength edge of the bandgap, as shown in Figure 12.

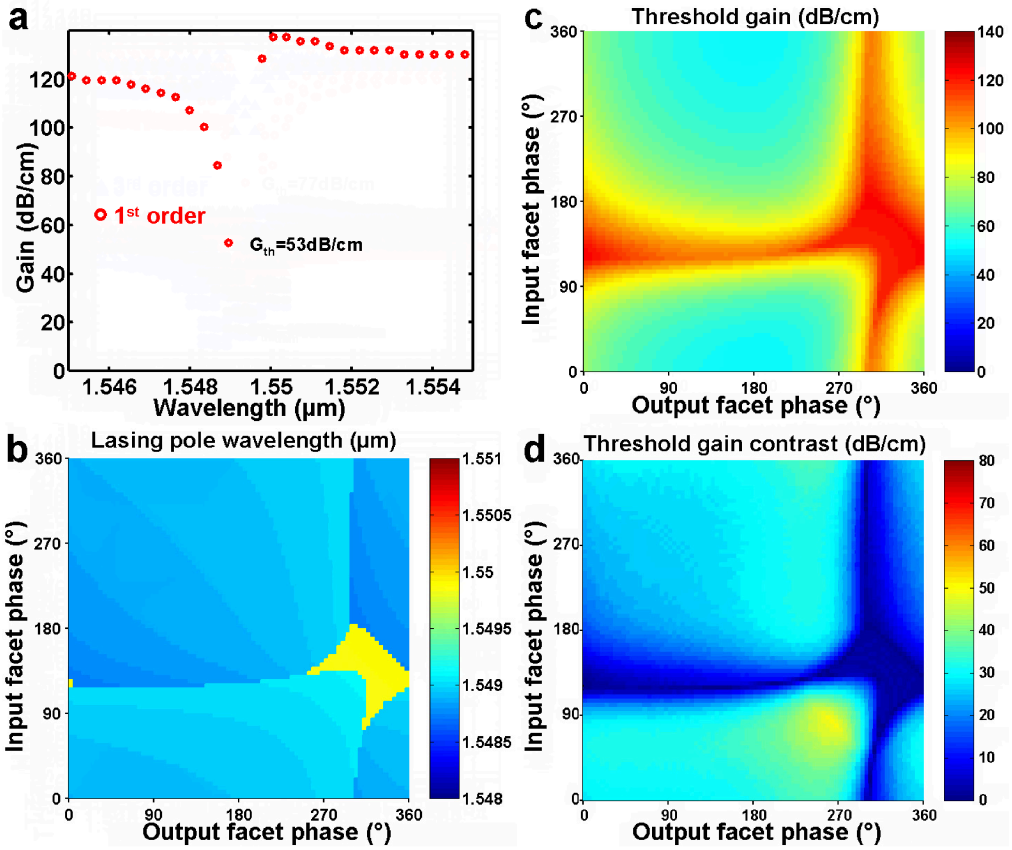


Figure 12. (**a**) Map of the position of the transmission matrix poles for a first-order 1 mm long complex index profile BG with $\Psi = 180°$ and refractive index modulation $\Delta n_{Re} = 0.002$ and $\Delta n_{Im} = 0.0004$. (**b**) Color map showing variation in the emission wavelength at the threshold gain level as a function of input and output facet termination. (**c**) Color map showing variation in the threshold gain level as a function of input and output facet termination. (**d**) Color map showing variation in the threshold gain contrast between the lowest pole and the immediately higher one as a function of input and output facet termination.

2.5. First-Order PT-Symmetric DFB Lasers ($\Psi = 90°$ or $\Psi = 270°$)

To study the behavior of a PT-symmetric (PTS) BG, a DFB laser with a complex refractive index profile grating where $\Delta n_{Re} = 0.002$ and $\Delta n_{Im} = 0.0004$ while $\Psi = 90°$ is considered below. Evidently, the pattern of the threshold gain color map in Figure 13c is overall very similar to that of the DFB dielectric grating, except that the absolute threshold gain values are much higher. The distribution as a function of wavelength of the transmission poles of this first-order 1 mm long DFB laser is shown in Figure 13a. This modeling was performed for one of the two optimal configurations of facet termination in terms of the lowest

threshold gain shown in Figure 13c with $\Phi_{in} = 305°$ and $\Phi_{out} = 145°$. This configuration approximately corresponds to the case where the dielectric grating BG begins and ends with $3\Lambda/8$ thickness nH layers, while metallic grating begins with a $\Lambda/8$ thickness gain layer and ends with a $\Lambda/8$ thickness metal absorption layer. Note that such a configuration has mirror and inversion symmetry for dielectric grating but only inversion symmetry for metallic grating. Thus, the combined grating also presents inversion symmetry.

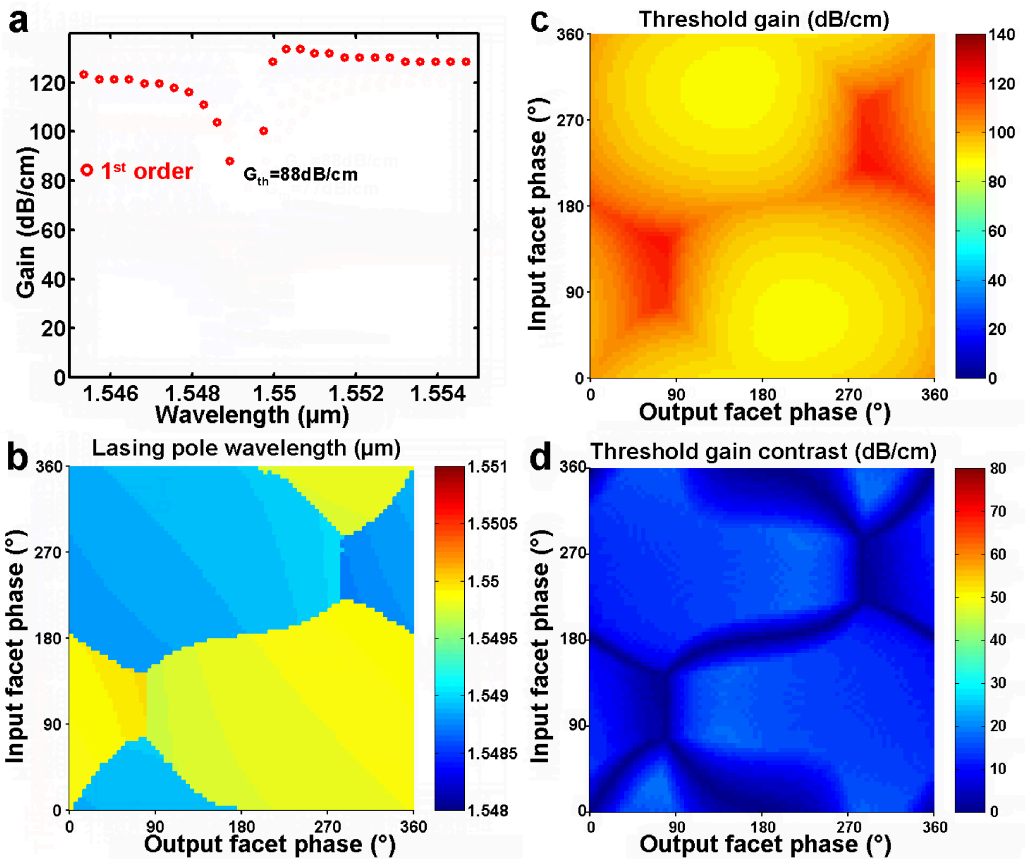


Figure 13. (**a**) Map of the position of the transmission matrix poles for a first-order 1 mm long PT-symmetric refractive index profile BG with $\Psi = 90°$ and refractive index modulation $\Delta n_{Re} = 0.002$ and $\Delta n_{Im} = 0.0004$. (**b**) Color map showing variation in the emission wavelength at the threshold gain level as a function of input and output facet termination. (**c**) Color map showing variation in the threshold gain level as a function of input and output facet termination. (**d**) Color map showing variation in the threshold gain contrast between the lowest pole and the immediately higher one as a function of input and output facet termination.

The onset of lasing at the lowest gain pole characterized by a threshold $G_{th} = 88$ dB/cm occurs at the short-wavelength edge of the bandgap. The gain contrast relative to the immediately higher pole is only 12 dB/cm. In this respect, the situation is comparable to that of dielectric-grating DFB lasers, but the threshold gain is nearly five times higher. It even exceeds that of metallic-grating DFB lasers by 10 dB/cm.

This result is entirely due to the unfavorable interaction for the phase shift $\Psi = 90°$ of the resonance phenomena in the dielectric grating and that of the absorption due to the metallic grating. For comparison, as shown in Figure 10b, the gain level of a bare PTS BG without end reflectivity is about 140 dB/cm lower than that of a similar bare metal-only grating. On the other hand, as explained above, the metal DFB laser yields better performance for two reasons: for operation at λ_{Br}, the spatial periodicity of the light intensity coincides with that of the grating, and under right-facet termination, there is less light absorption. This is not the case for PTS DFB lasers, where the distribution of poles

is largely similar to that of dielectric BGs since $\Delta n_{\mathrm{Im}} = << \Delta n_{\mathrm{Re}}$. However, in terms of remedying this situation, it is impossible to further increase the value Δn_{Im} in order to avoid even-higher absorption losses. A more detailed discussion on the optimal level of absorption losses is presented in Section S1 of the SM.

The configuration where the dielectric and metallic gratings are shifted by $\varphi = 270°$ yields similar results, as shown in Figure 14. It therefore appears that the DFB laser with a PTS BG corresponds to the worst case in our study. Its overall spectral behavior is essentially determined by the dielectric grating. The contribution of the $\Psi = 90°$ or $\Psi = 270°$ phase-shifted metallic grating is reduced to increase absorption losses, resulting in a much higher level of threshold gain. In the overall balance of the amplification process leading to the onset of lasing, the effect of increased asymmetric reflection in one direction is counterbalanced by reduced reflection in the opposite direction.

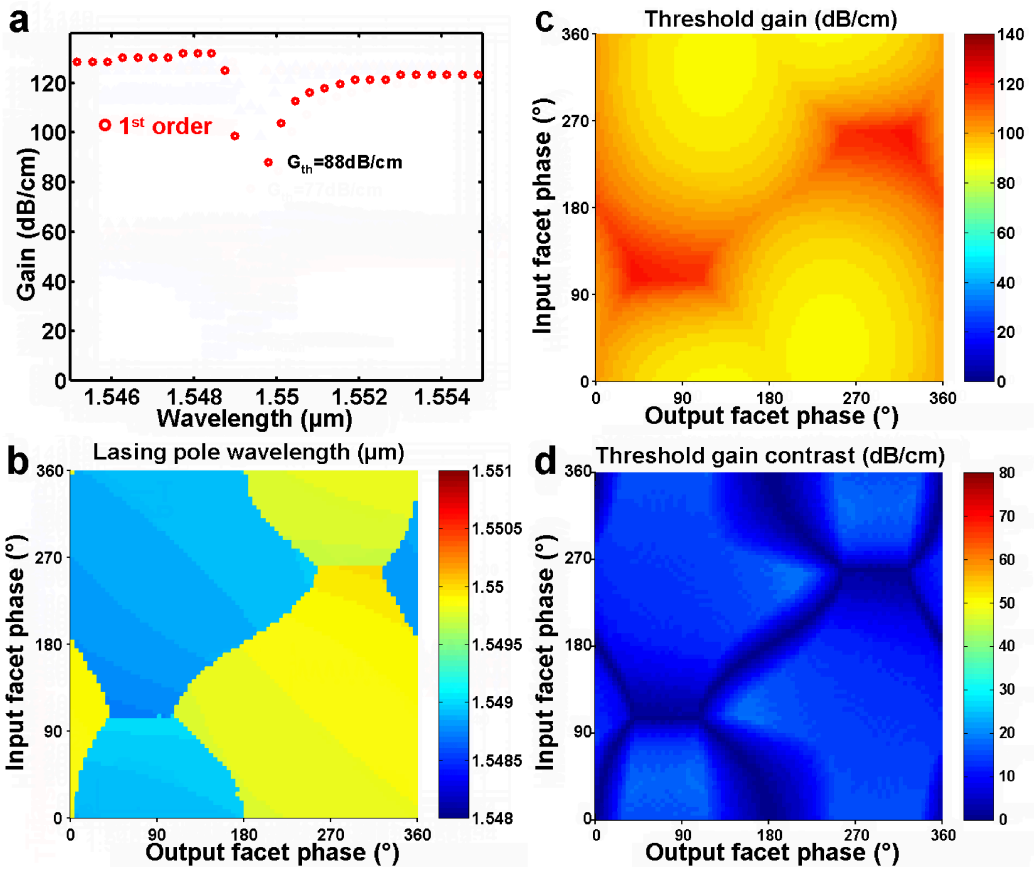


Figure 14. (**a**) Map of the position of the transmission matrix poles for a first-order 1 mm long PT-symmetric refractive index profile BG with $\Psi = 270°$ and refractive index modulation $\Delta n_{\mathrm{Re}} = 0.002$ and $\Delta n_{\mathrm{Im}} = 0.0004$. (**b**) Color map showing variation in the emission wavelength at the threshold gain level as a function of input and output facet termination. (**c**) Color map showing variation in the threshold gain level as a function of input and output facet termination. (**d**) Color map showing variation in the threshold gain contrast between the lowest pole and the immediately higher one as a function of input and output facet termination.

However, the positive point is that this example, as well as the previous one for the CC-DFB lasers, shows that the combined action of the dielectric and metallic gratings indeed matters, but it must be employed in the right way. To this end, the two issues that need to be addressed are noted below:

- Exploit the resonant wavelength-selection mechanism characteristic of the metallic grating DFB; the emission wavelength should occur at λ_{Br}.
- Increase the contribution of PTS BG asymmetric reflection to the overall balance of the amplification process in the DFB laser cavity.

The solution to these issues is presented in the next section.

3. Optimal Design of First-Order CC-DFB Lasers with AR/HR Coatings

3.1. Toward Unveiling PT-Symmetry Potential for DFB Laser Applications

One of the major conclusions presented in the previous section is that combined modulation of the real and imaginary parts of the grating's refractive index profile can effectively improve DFB lasers, particularly regarding single-mode operation robustness, threshold gain levels, and gain contrast relative to the immediately higher-order laser pole. This is especially true for CC-DFB lasers, where the dielectric and metallic gratings are either in-phase ($\Psi = 0°$) or out-of-phase ($\Psi = 180°$). In contrast, for PT-symmetric configurations ($\Psi = 90°$ or $\Psi = 270°$), reflection asymmetry, which is intended to further enhance DFB laser performance through an additional narrow-band amplification mechanism, is compromised by facet reflection. Proposed solutions to this issue involve aligning the emission wavelength with λ_{Br} and increasing asymmetric reflection's contribution to the overall amplification process.

The conventional approach to achieving dielectric-grating DFB laser emission at λ_{Br} involves inserting a quarter-wave phase-shift section with a length of $\Lambda/2$ in the middle of the laser cavity [2]. For $\lambda/4$ phase-shifted DFB lasers with low facet reflectivity ($R < 1\%$), emission occurs exactly at the Bragg wavelength. Although a similar approach based on introducing a grating defect that acts as a phase shifter within a "head-to-tail" arrangement using PT-symmetric BG is theoretically feasible, it presents certain drawbacks. The most significant issue is that low facet reflectivity is required to avoid laser performance degradation. However, the concomitant increase in cavity mirror losses leads to a rise in threshold gain. This situation is highly disadvantageous, given that metal absorption losses also contribute to increasing the threshold gain. It is therefore necessary to consider a solution in which the mirror losses determined by the product of the left- and right-facet reflectivities $R_L R_R$ remains unchanged.

As mentioned in the previous section, an additional π phase shift occurs when light from the less dense optical material is reflected at the interface with a denser optical material. This phase shift is the same as that produced by the $\Lambda/2$ section. The proposed solution therefore consists of using high-reflectivity and anti-reflective (HR/AR) facet coatings while keeping $R_{AR}R_{HR} = R_L R_R$. To model such a structure, a simplified design version was used, with $R_{AR} = 7.9\%$ and $R_{HR} = 99.9\%$. Here, the role of the AR coating plays a semi-infinite hypothetical optical material with a refractive index $n = 1.81$, while for the HR coating a semi-infinite hypothetical optical material with a refractive index $n = 9999$. Some results obtained with a realistic AR/HR design are presented in Section S2 of the SM. To verify the validity of the considered approach, the proposed concept is first applied to the case of the dielectric grating DFB laser.

3.2. First-Order Dielectric Grating DFB Laser with AR/HR Facet Coatings

The distribution as a function of wavelength of the transmission poles for a 1 mm long AR/HR-coated DFB laser for which only the real part of the refractive index $\Delta n_{Re} = 0.002$ has been modified is shown in Figure 15a. This modeling was performed for the optimal configuration of facet termination in terms of the lowest threshold gain shown in Figure 15c with $\Phi_{AR} = 180°$ and $\Phi_{HR} = 0°$. For this case, the lowest pole, at $G_{th} = 1.4$ dB/cm, corresponds to the onset of laser emission exactly at the Bragg wavelength. The gain contrast

relative to the immediately higher gain pole is 27 dB/cm. This gain contrast is more than twice that of the uncoated dielectric grating DFB laser and contributes to ensuring much-more-robust single-frequency laser emission.

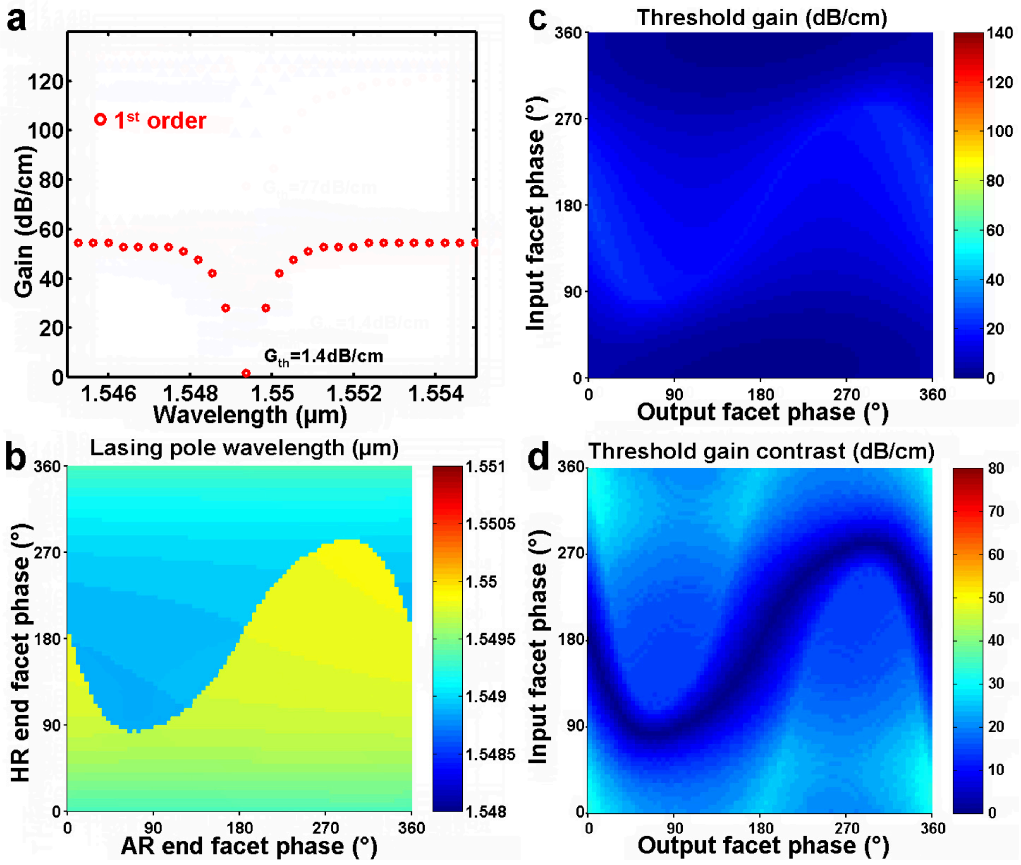


Figure 15. (**a**) Map of the position of the transmission matrix poles for a first-order 1 mm long dielectric BG with AR/HR coatings and refractive index modulation $\Delta n_{\mathrm{Re}} = 0.002$. (**b**) Color map showing variation in the emission wavelength at the threshold gain level as a function of input and output facet termination. (**c**) Color map showing variation in the threshold gain level as a function of input and output facet termination. (**d**) Color map showing variation in the threshold gain contrast between the lowest pole and the immediately higher one as a function of input and output facet termination.

Figure 15b is a color map showing the emission wavelength for the lowest-gain pole as a function of facet variation. Evidently, the emission wavelength almost does not depend on Φ_{AR} facet termination at all when $\Phi_{\mathrm{HR}} \in [-80°, 80°]$. This is equivalent to a laser yield of about 45%. The results obtained thus fully validate the relevance of the approach considered, which we subsequently applied to DFB lasers with PT-symmetry.

3.3. First-Order PT-Symmetric DFB Lasers with AR/HR Facet Coatings ($\Psi = 90°$ or $\Psi = 270°$)

As noted in the previous section, a PTS DFB laser with a complex refractive index profile grating where $\Delta n_{\mathrm{Re}} = 0.002$ and $\Delta n_{\mathrm{Im}} = 0.0004$ is considered below. The concept used to improve reflection asymmetry is illustrated in Figure 16a. It consists of ensuring there is higher reflectivity of the BG towards the HR-coated facet of the laser and lower reflectivity towards the AR-coated one. This corresponds to a phase shift $\Psi = 90°$ between the real and imaginary parts of refractive index modulation by considering as the reference light incidence from the left (AR) end of the laser. Even though the grating does not correspond to the condition of perfect PT-symmetry, where $\Delta n_{\mathrm{Re}} = \Delta n_{\mathrm{Im}}$, the degree of reflection asymmetry is still pronounced. The spectral response of the BG considered in this

case study, but without reflectivity of the facets and operating at a gain level just enough to compensate for the absorption losses, is shown in Figure 16b. Evidently, the reflectivity toward the HR laser end (right facet) is more than twice that toward the AR one (left facet). As a result, an increase in photon lifetime in the laser cavity that leads to a reduction in the threshold gain level can be expected. The modeling results presented below fully validate this approach.

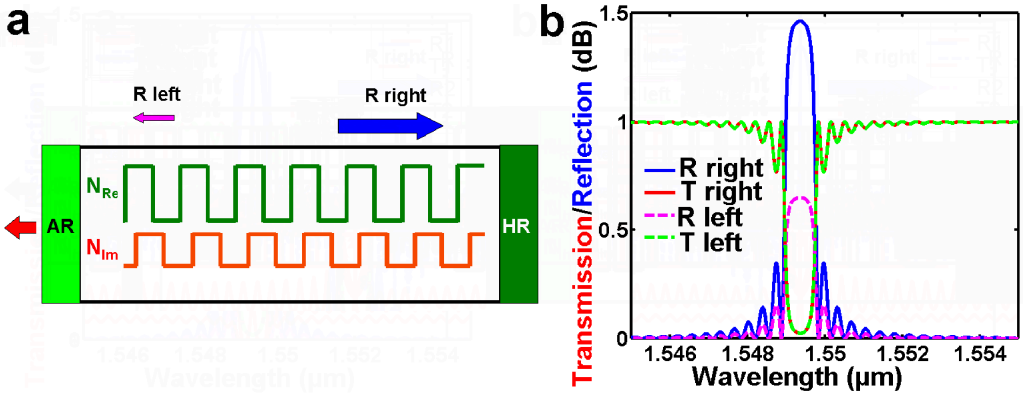


Figure 16. (**a**) Schematic depicting the AR/HR-coated DFB laser with a complex index profile BG where $\Psi = 90°$. The red arrow indicates the direction of laser light emission. Asymmetric reflectivity toward the left and right propagation directions is indicated by blue and magenta arrows, respectively. (**b**) The spectral response of the considered complex profile BG without facet reflectivity. Note that outside the bandgap, the transmission is equal to unity because of exact absorption loss compensation by gain.

The distribution as a function of wavelength of the transmission poles for a 1 mm long AR/HR-coated PT-symmetric DFB laser is shown in Figure 17a. This modeling was performed for the optimal configuration of facet termination in terms of the lowest threshold gain shown in Figure 17c with $\Phi_{AR} = 180°$ and $\Phi_{HR} = 0°$. In this case, the lowest pole, at G_{th} = 26.4 dB/cm, corresponds to the onset of laser emission exactly at the Bragg wavelength. As shown in Figure 17a, the contrast of the gain level relative to the immediately higher gain pole reaches 70 dB/cm. Such high gain is expected to facilitate extremely robust single-frequency laser operation. This also suggests increased tolerance of laser operation with respect to parasitic optical feedback and potentially isolator-free operation.

A color map showing the emission wavelength for the lowest-gain pole as a function of facet variation is shown in Figure 17b. Evidently, the emission wavelength almost does not depend on Φ_{AR} facet termination at all when $\Phi_{HR} \in [-110°, 110°]$. This is equivalent to a laser yield of about 62%. The yield can be further increased by using an adjustable integrated or external tunable cavity similar to that used in [17] to provide necessary HR end phase correction. Note the unidirectional trend appearing in these results; it is more pronounced than in the other cases, as the facets here serve to reinforce the phenomenon.

Overall, the parameters of the PT-symmetric DFB laser are superior to those of the dielectric grating DFB laser, except for the higher threshold gain, which, as an absolute value, is still low enough. For the sake of comparison, the PTS laser corresponding to the opposite configuration when $\Psi = 270°$ is also considered below.

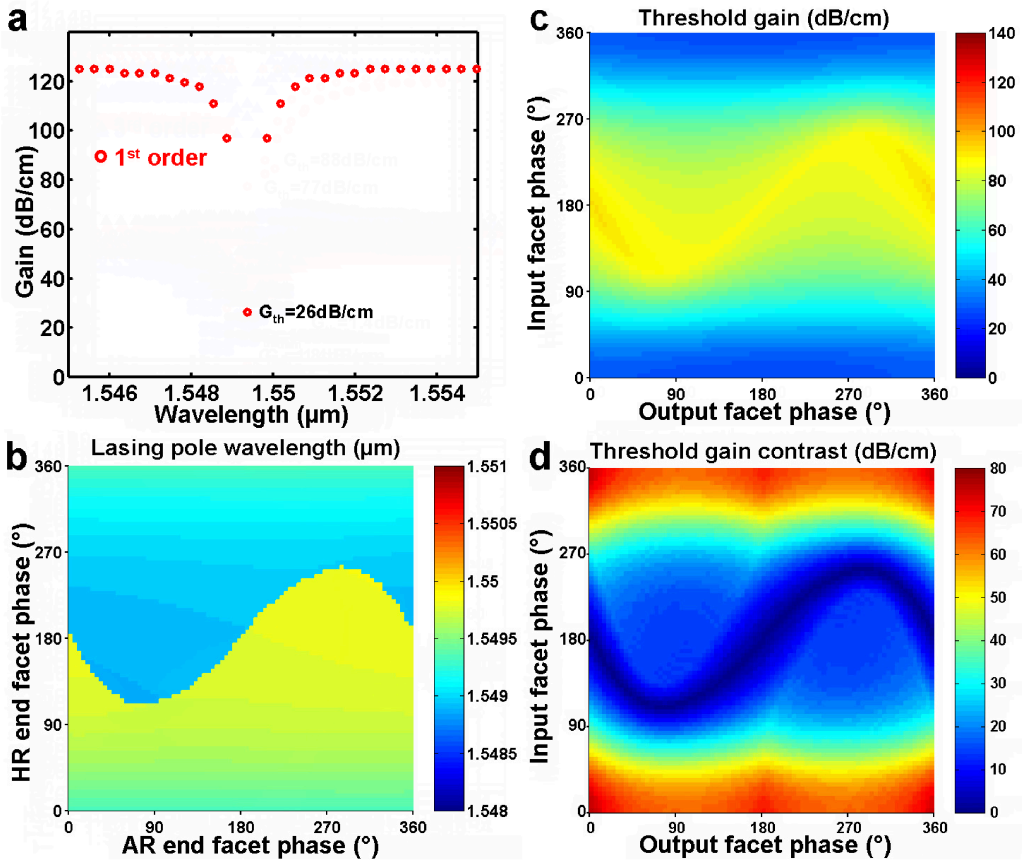


Figure 17. (**a**) Map of the position of the transmission matrix poles for a first-order 1 mm long PT-symmetric refractive index profile BG with AR/HR coatings where $\Psi = 90°$ and refractive index modulation $\Delta n_{Re} = 0.002$ and $\Delta n_{Im} = 0.0004$. (**b**) Color map showing variation in the emission wavelength at the threshold gain level as a function of input and output facet termination. (**c**) Color map showing variation in the threshold gain level as a function of input and output facet termination. (**d**) Color map showing variation in the threshold gain contrast between the lowest pole and the immediately higher one as a function of input and output facet termination.

The distribution as a function of wavelength of the transmission poles for a 1 mm long AR/HR-coated PT-symmetric DFB laser when $\Psi = 270°$ is shown in Figure 18a. This modeling was performed for one of the two optimal configurations of facet termination in terms of the lowest threshold gain shown in Figure 18c with $\Phi_{AR} = 180°$ and $\Phi_{HR} = 252°$. In this case, the onset of laser emission at the lowest pole with $G_{th} = 88$ dB/cm occurs at the long-wavelength edge of the bandgap. The gain level contrast with respect to the next lowest pole located at a wavelength above the BG bandgap is quite modest, being about 15 dB/cm.

A color map showing the emission wavelengths for the poles with the lowest gain as a function of facet variation is shown in Figure 18b. Evidently, the blue region, mainly located in the left half of the map, corresponds to wavelength emission below the bandgap. The yellow region, located essentially in the right half of the map, corresponds to wavelength emission above the bandgap. The overall behavior is very similar to that of uncoated-facet PT-symmetric DFB lasers with $\Psi = 270°$. These results show that it is indeed possible to exploit reflection asymmetry, which is a characteristic feature of the PT-symmetric BG, provided the design is carried out correctly.

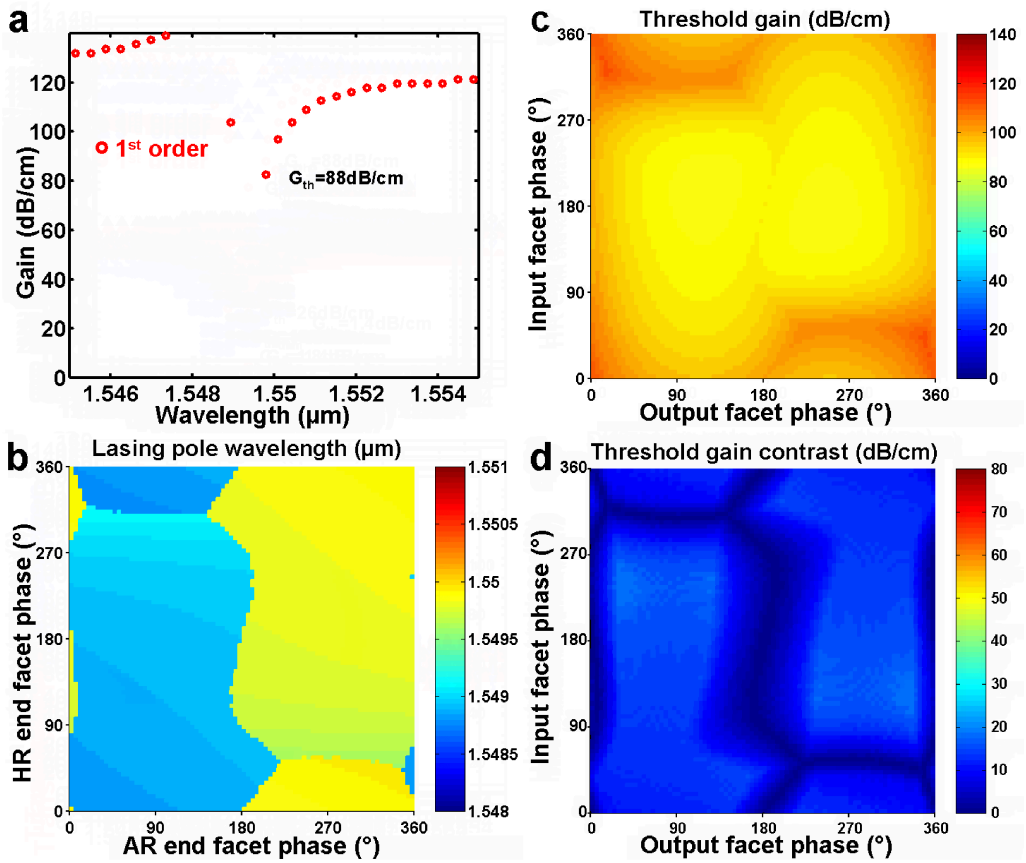


Figure 18. (**a**) Map of the position of the transmission matrix poles for first- and third-order 1 mm long PT-symmetric refractive index profile BGs with AR/HR coatings where $\Psi = 270°$ and refractive index modulation $\Delta n_{Re} = 0.002$ and $\Delta n_{Im} = 0.0004$. (**b**) Color map showing variation in the emission wavelength at the threshold gain level as a function of input and output facet termination. (**c**) Color map showing variation in the threshold gain level as a function of input and output facet termination. (**d**) Color map showing variation in the threshold gain contrast between the lowest pole and the immediately higher one as a function of input and output facet termination.

3.4. First-Order CC-DFB Lasers ($\Psi = 0°$ or $\Psi = 180°$) with AR/HR Facet Coatings

To ensure completeness of the study, the results for CC-DFB lasers and metallic grating DFB lasers are also presented below. The distribution as a function of wavelength of the transmission poles of a first-order 1 mm long CC-DFB laser where $\Psi = 0°$ is shown in Figure 19a. This modeling was performed for the optimal configuration of facet termination in terms of the lowest threshold gain shown in Figure 19c with $\Phi_{AR} = 200°$ and $\Phi_{HR} = 79°$. This configuration corresponds to the case where the BG begins and ends with a complete period corresponding to a higher index nH and a metal-free region. In this case, the onset of laser emission at the lowest pole with $G_{th} = 37$ dB/cm occurs at the long-wavelength edge of the bandgap. The blue-green region located outside that delimited by yellow in Figure 19c, which corresponds to the lower threshold gain, represents approximately 94% of the total area of the color map. This feature would result in high yield for lasers, with acceptable performance. The performance improvement with respect to the uncoated case is also remarkable, although it is less impressive relative to that for PTS DFB laser. However, the reasons for this improvement are yet to be understood.

The case where the dielectric and metallic gratings are in antiphase ($\Psi = 180°$) yields similar results, except that the emission now occurs at the short-wavelength edge of the bandgap.

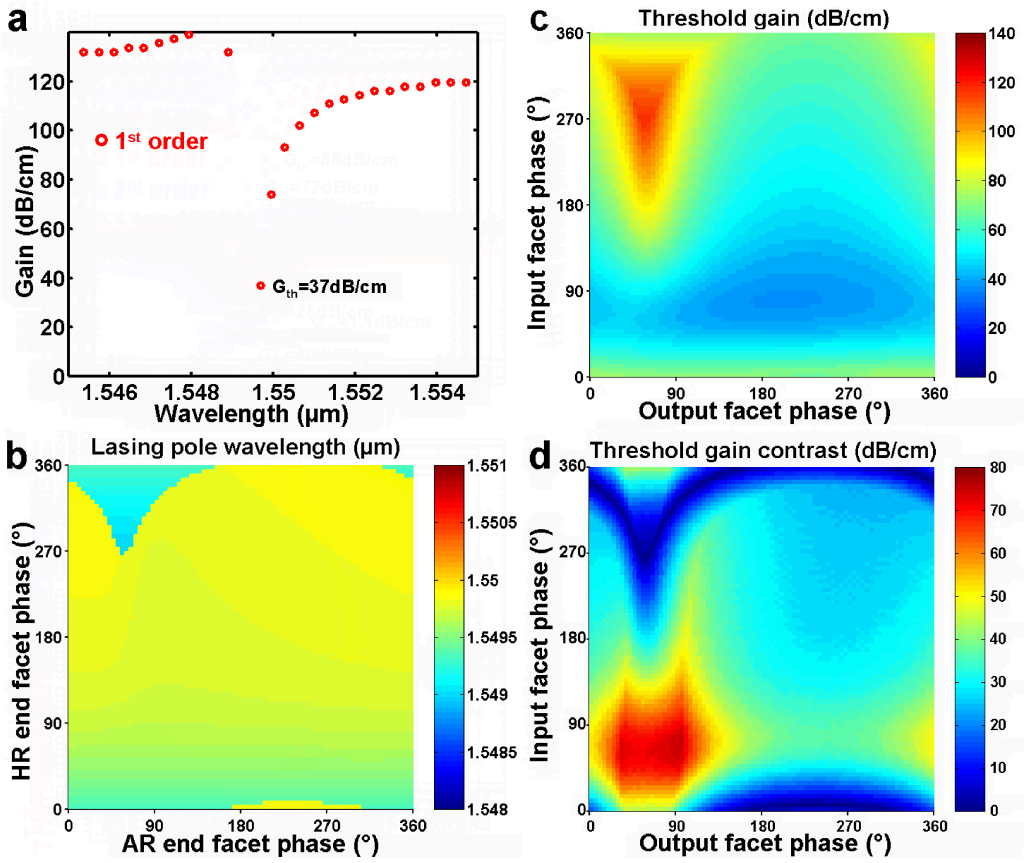


Figure 19. (**a**) Map of the position of the transmission matrix poles for a first-order 1 mm long complex index profile BG with AR/HR coatings where $\Psi = 0^\circ$ and refractive index modulation $\Delta n_{Re} = 0.002$ and $\Delta n_{Im} = 0.0004$. (**b**) Color map showing variation in the emission wavelength at the threshold gain level as a function of input and output facet termination. (**c**) Color map showing variation in the threshold gain level as a function of input and output facet termination. (**d**) Color map showing variation in the threshold gain contrast between the lowest pole and the immediately higher one as a function of input and output facet termination.

3.5. First-Order Metallic Grating DFB Laser with AR/HR Facet Coatings

The distribution as a function of wavelength of the transmission poles for a first-order 1 mm long metallic grating DFB laser for which only the imaginary part of the refractive index ($\Delta n_{Im} = 0.0004$) has been modulated is shown in Figure 20a. This modeling was performed for the optimal configuration of facet termination in terms of the lowest threshold gain shown in Figure 20c with $\Phi_{AR} = 90^\circ$ and $\Phi_{HR} = 90^\circ$. This corresponds to the configuration where the BG from the AR-coated facet begins with a quarter period of metal-free region, while on the HR-coated facet, things end with a quarter period with a metallic region. In this case, the onset of laser emission at the lowest pole with $G_{th} = 70$ dB/cm occurs at λ_{Br}. The gain level contrast with respect to the next-lowest poles is ~54 dB/cm. Although this type of laser also shows some improvement over the uncoated case, this improvement is considerably more modest relative to the rest of the DFB lasers considered in this study.

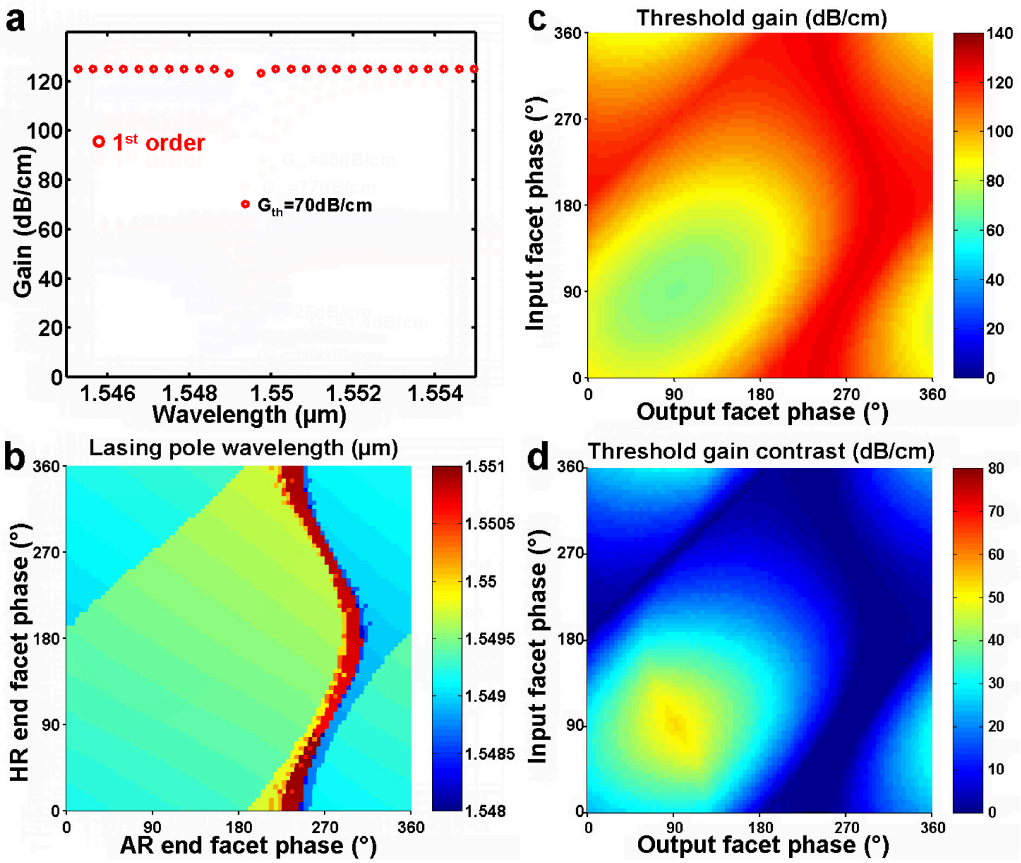


Figure 20. (**a**) Map of the position of the transmission matrix poles for a first-order 1 mm long metallic BG with AR/HR coatings and refractive index modulation $\Delta n_{\mathrm{Im}} = 0.0004$. (**b**) Color map showing variation in the emission wavelength at the threshold gain level as a function of input and output facet termination. (**c**) Color map showing variation in the threshold gain level as a function of input and output facet termination. (**d**) Color map showing variation in the threshold gain contrast between the lowest pole and the immediately higher one as a function of input and output facet termination.

4. Summary and Outlook

This work focused on the optimal design of CC-DFB lasers, with an emphasis on aspects related to the symmetry properties of the BG that account for the phase at the facet end. According to the ways in which gain and loss are modulated in the light propagation direction, we conducted a comparative modeling study of different types of DFB lasers, including conventional dielectric BG DFB, metallic grating DFB, and complex-coupled DFB lasers with phase-shifted dielectric and metallic gratings. The influences of the phase shift between the two gratings and of the facet boundary conditions were examined in terms of threshold gain levels and the gain contrast between the lowest-gain mode and the immediately higher-order one.

A major conclusion of this modeling study is that the combined modulation of the real and imaginary parts of the grating refractive index profile can indeed improve DFB lasers, in terms of increasing the robustness of single-frequency operation, reducing the gain threshold, and improving gain contrast between the lowest lasing pole and the immediately higher one. This is particularly the case for complex-coupled DFB lasers where the dielectric and metallic gratings are either in-phase or in antiphase. In contrast, for PT-symmetric configurations, reflection asymmetry intended to further enhance DFB laser performance through an additional narrow-band amplification mechanism is compromised by facet reflection.

To solve this problem, it is necessary to find a way to make the lasing wavelength correspond to the Bragg wavelength and enhance the contribution of asymmetric reflection to the overall balance of the amplification process. The solution we propose consists of using high-reflectivity and anti-reflective (HR/AR) facet coatings. The modeling results for this design show a low-enough threshold gain level of 26 dB/cm, corresponding to the onset of laser emission exactly at the Bragg wavelength. The contrast of the gain level relative to the immediately higher gain pole reaches 72 dB/cm. Such a high gain contrast should allow for extremely robust single-frequency laser operation. This also suggests increased tolerance of laser operation with respect to parasitic optical feedback, potentially resulting in isolator-free operation.

Supplementary Materials: The following supporting information can be downloaded at: https://www.mdpi.com/article/10.3390/photonics13100934/s1. References [11,17–19] are cited in the Supplementary Materials.

Author Contributions: Conceptualization, Y.L., Y.E.D., H.B., A.R. and A.L.; methodology, Y.L., Y.E.D., H.B., A.R. and A.L.; software, Y.L., Y.E.D. and A.L.; validation, Y.L., Y.E.D., H.B., A.R. and A.L.; formal analysis, H.B., A.R. and A.L.; investigation, Y.L., Y.E.D., H.B., A.R. and A.L.; resources, A.R. and A.L.; data curation, Y.L., Y.E.D. and A.L.; writing—original draft preparation, Y.L., Y.E.D., H.B., A.R. and A.L.; writing—review and editing, Y.E.D., H.B. and A.L.; visualization, Y.L., Y.E.D. and H.B.; supervision, H.B., A.R. and A.L.; project administration, A.R. and A.L.; funding acquisition, Y.L. and A.L. All authors have read and agreed to the published version of the manuscript.

Funding: This work was partially funded by the French Agence Nationale pour la Recherche (project "PARTISYMO", contract number N° ANR-18-CE24-0024).

Data Availability Statement: The data underlying the results presented in this paper are not publicly available at this time but may be obtained from the corresponding author upon reasonable request.

Acknowledgments: Y.L. acknowledges the funding provided by the China Scholarship Council (grant number 201906750021). This work was performed within the C2N micro nanotechnologies platforms and was partly supported by the RENATECH network and the General Council of Essonne.

Conflicts of Interest: The authors declare there are no conflicts of interest.

References

1. Available online: https://dataintelo.com/report/distributed-feedback-laser-market (accessed on 20 July 2026).
2. David, K.; Morthier, G.; Vankwikelberge, P.; Baets, R.G.; Wolf, T.; Borchert, B. Gain-coupled DFB lasers versus index-coupled and phase shifted DFB lasers: A comparison based on spatial hole burning corrected yield. *IEEE J. Quantum Electron.* **1991**, *27*, 1714–1723. [CrossRef] [PubMed]
3. Kinoshita, J.; Matsumoto, K. Yield analysis of SLM DFB lasers with an axially-flattened internal field. *IEEE J. Quantum Electron.* **1989**, *25*, 1324–1332. [CrossRef] [PubMed]
4. Nakamura, K.; Miyamura, S.; Yaegashi, H. Optical feedback-tolerant gain-coupled DFB lasers for isolator-free modules in the access networks. *IEICE Trans. Electron.* **2010**, *93*, 1165–1171. [CrossRef]
5. Aliannezhadi, M.; Shahshahani, F.; Ahmadi, V. Improved performance of complex gain-coupled DFB laser by using tapered grating structure. *Opt. Quantum Electron.* **2012**, *44*, 1–16. [CrossRef]
6. Kamp, M.; Hofmann, J.; Schäfer, F.; Reinhard, M.; Fischer, M.; Bleuel, T.; Reithmaier, J.P.; Forchel, A. Lateral coupling–a material independent way to complex coupled DFB lasers. *Opt. Mater.* **2001**, *17*, 19–25. [CrossRef]
7. Nakano, Y.; Deguchi, Y.; Ikeda, K.; Luo, Y.; Tada, K. Reduction of excess intensity noise induced by external reflection in a gain-coupled distributed feedback semiconductor laser. *IEEE J. Quantum Electron.* **1991**, *27*, 1732–1735. [CrossRef] [PubMed]
8. David, K.; Buus, J.; Morthier, G.; Baets, R. Coupling coefficients in gain-coupled DFB lasers: Inherent compromise between coupling strength and loss. *IEEE Photonics Technol. Lett.* **1991**, *3*, 439–441. [CrossRef]
9. Petermann, K. External optical feedback phenomena in semiconductor lasers. *IEEE J. Sel. Top. Quantum Electron.* **1995**, *1*, 480–489. [CrossRef]
10. Benisty, H.; de la Perrière, V.B.; Ramdane, A.; Lupu, A. Parity-time Symmetric gratings in 1550 nm Distributed-Feedback lasers diodes: Insight on device design rules. *J. Opt. Soc. Am. B* **2021**, *38*, C168–C174. [CrossRef]

11. Brac de la Perrière, V.; Gaimard, Q.; Benisty, H.; Ramdane, A.; Lupu, A. Electrically injected parity-time symmetric DFB lasers for telecom applications. *Nanophotonics* **2021**, *10*, 1309–1317. [CrossRef]
12. Ke, C.; Li, X.; Xi, Y. Parity-time symmetric complex-coupled distributed feedback laser with excellent immunity to external optical feedback. *AIP Adv.* **2017**, *7*, 035010. [CrossRef]
13. Hao, T.; Cheben, P.; Schmid, J.H.; Berini, P. Parity-time and anti-parity-time states of Bragg gratings and their representation in spherical coordinates. *Opt. Express* **2024**, *32*, 45521–45530. [CrossRef]
14. Akhter, M.N.; Ivars, S.B.; Botey, M.; Herrero, R.; Staliunas, K. Non-Hermitian Mode Cleaning in Periodically Modulated Multimode Fibers. *Phys. Rev. Lett.* **2023**, *131*, 043604. [CrossRef] [PubMed]
15. Akhter, M.N.; Botey, M.; Herrero, R.; Staliunas, K. Non-Hermitian mode management in periodically modulated waveguide amplifiers. *APL Photonics* **2024**, *9*, 106115. [CrossRef]
16. Staliunas, K. Normal forms of unidirectional coupling in quasi-phase-matched non-Hermitian systems. *arXiv* **2026**. [CrossRef]
17. Liang, Y.; Coudevylle, J.-R.; Benisty, H.; Ramdane, A.; Lupu, A. Strong Laser Emission Modulation by Coherent Perfect Absorption Inside Complex-Coupled Distributed Feedback Laser Diodes. *Small* **2025**, *21*, 2570003. [CrossRef] [PubMed]
18. Dubrovina, N.; Liang, Y.; Gaimard, Q.; Brac de la Perrière, V.; Merghem, K.; Benisty, H.; de Lustrac, A.; Ramdane, A.; Lupu, A. Electrically injected metamaterial grating DFB laser exploiting an ultra−high Q Electromagnetic Induced Transparency resonance for spectral selection. *Adv. Funct. Mater.* **2024**, *34*, 2405912. [CrossRef]
19. Le Gall, F.; Mottet, S.; Devoldere, N.; Landreau, J. External cavity laser for DWDM access network. In Proceedings of the 24th European Conference on Optical Communication, Madrid, Spain, 20–24 September 1998; pp. 285–286. [CrossRef]

Disclaimer/Publisher's Note: The statements, opinions and data contained in all publications are solely those of the individual author(s) and contributor(s) and not of MDPI and/or the editor(s). MDPI and/or the editor(s) disclaim responsibility for any injury to people or property resulting from any ideas, methods, instructions or products referred to in the content.